NAVAL POSTGRADUATE SCHOOL

MONTEREY, CALIFORNIA

THESIS

SHIELDING REQUIREMENTS FOR AN ENERGY-RECOVERY LINAC FREE ELECTRON LASER

by

Robert E. Peterson

December 2011

Thesis Co-Advisors: William B. Colson
Keith Cohn

Approved for public release; distribution is unlimited

THIS PAGE INTENTIONALLY LEFT BLANK

REPORT DOCUMENTATION PAGE			Form Approved OMB No. 0704–0188
Public reporting burden for this collection of information is estimated to average 1 hour per response, including the time for reviewing instruction, searching existing data sources, gathering and maintaining the data needed, and completing and reviewing the collection of information. Send comments regarding this burden estimate or any other aspect of this collection of information, including suggestions for reducing this burden, to Washington headquarters Services, Directorate for Information Operations and Reports, 1215 Jefferson Davis Highway, Suite 1204, Arlington, VA 22202–4302, and to the Office of Management and Budget, Paperwork Reduction Project (0704–0188) Washington DC 20503.			
1. AGENCY USE ONLY *(Leave blank)*	**2. REPORT DATE** December 2011	**3. REPORT TYPE AND DATES COVERED** Master's Thesis	
4. TITLE AND SUBTITLE Shielding Requirements for an Energy-Recovery Linac Free Electron Laser		**5. FUNDING NUMBERS**	
6. AUTHOR(S) Robert E. Peterson			
7. PERFORMING ORGANIZATION NAME(S) AND ADDRESS(ES) Naval Postgraduate School Monterey, CA 93943–5000		**8. PERFORMING ORGANIZATION REPORT NUMBER**	
9. SPONSORING /MONITORING AGENCY NAME(S) AND ADDRESS(ES) N/A		**10. SPONSORING/MONITORING AGENCY REPORT NUMBER**	
11. SUPPLEMENTARY NOTES The views expressed in this thesis are those of the author and do not reflect the official policy or position of the Department of Defense or the U.S. Government. IRB Protocol number _____N/A_____.			
12a. DISTRIBUTION / AVAILABILITY STATEMENT Approved for public release; distribution is unlimited		**12b. DISTRIBUTION CODE** A	

13. ABSTRACT (maximum 200 words)

Many Free Electron Lasers (FELs) utilize high current, high energy electron beams. Inevitably, a small fraction of the electrons in the beam will exist outside the core beam; these electrons are referred to as beam halo. The halo electrons will travel down an FEL's transport system with the core electrons; any portion of those halo electrons that intercept transport system components can generate radiation that is harmful to the operating personnel. The amount of shielding that is required to keep personnel safe from radiation exposure is evaluated as a function of the lost halo current. Using the modeling software FLUKA, an analysis is presented describing the amount of necessary shielding for a given shielding material.

14. SUBJECT TERMS Free Electron Laser, Radiation Shielding, Halo			**15. NUMBER OF PAGES** 109
			16. PRICE CODE
17. SECURITY CLASSIFICATION OF REPORT Unclassified	**18. SECURITY CLASSIFICATION OF THIS PAGE** Unclassified	**19. SECURITY CLASSIFICATION OF ABSTRACT** Unclassified	**20. LIMITATION OF ABSTRACT** UU

NSN 7540–01–280–5500 Standard Form 298 (Rev. 2–89)
Prescribed by ANSI Std. 239–18

THIS PAGE INTENTIONALLY LEFT BLANK

Approved for public release; distribution is unlimited

SHIELDING REQUIREMENTS FOR AN ENERGY-RECOVERY LINAC FREE ELECTRON LASER

Robert E. Peterson
Lieutenant, United States Navy
B.S., M.S., New School University, 2001
B.S., North Carolina State University, 2003

Submitted in partial fulfillment of the
requirements for the degree of

MASTER OF SCIENCE IN PHYSICS

from the

NAVAL POSTGRADUATE SCHOOL
December 2011

Author: Robert E. Peterson

Approved by: William B. Colson
Thesis Co-Advisor

Keith Cohn
Thesis Co-Advisor

Andrés Larraza
Chair, Department of Physics

THIS PAGE INTENTIONALLY LEFT BLANK

ABSTRACT

Many Free Electron Lasers (FELs) utilize high current, high energy electron beams. Inevitably, a small fraction of the electrons in the beam will exist outside the core beam; these electrons are referred to as beam halo. The halo electrons will travel down an FEL's transport system with the core electrons; any portion of those halo electrons that intercept transport system components can generate radiation that is harmful to the operating personnel. The amount of shielding that is required to keep personnel safe from radiation exposure is evaluated as a function of the lost halo current. Using the modeling software FLUKA, an analysis is presented describing the amount of necessary shielding for a given shielding material.

THIS PAGE INTENTIONALLY LEFT BLANK

TABLE OF CONTENTS

LIST OF FIGURES

THIS PAGE INTENTIONALLY LEFT BLANK

LIST OF TABLES

THIS PAGE INTENTIONALLY LEFT BLANK

LIST OF SYMBOLS

a	dimensionless optical field strength
$\vec{A}$	vector potential
B	magnitude of the undulator magnetic field
$\vec{B}$	vector sum of the undulator and optical magnetic fields
$\vec{B}_0$	optical magnetic field
$\vec{B}_U$	undulator magnetic field
c	speed of light
e	charge of an electron
E	magnitude of the optical electric field
$\vec{E}_0$	optical electric field
G	optical gain
j	dimensionless electron current
$J_\perp$	transverse current density
k	optical wave number
k_0	undulator magnetic wave number
K	undulator parameter
L	undulator length
m	electron mass
N	number of undulator periods
q	bunch charge
$\vec{r}$	position vector
r_b	electron beam radius
t	time
v_z	electron longitudinal velocity
w	optical mode cross section radius
w_0	optical mode waist
x	undulator transverse coordinate parallel to the magnetic field
y	undulator transverse coordinate perpendicular to the magnetic field
z	undulator longitudinal coordinate

Z_0	Raleigh length
$\vec{\beta}$	non-dimensional electron velocity
$\beta_\perp$	transverse component of
β_z	longitudinal component of
γ	Lorentz factor
$\hat{\varepsilon}$	polarization vector $(-i,1,0)$
ε_n	transverse emittance parameter
ς	electron phase
η	undulator extraction
θ_b	electron beam divergence
λ	optical wavelength
λ_0	length of undulator period
ν	dimensionless phase velocity
σ	dimensionless electron beam radius
ρ	electron density
τ	dimensionless time
φ	initial optical phase
ψ	optical phase
ω	optical frequency
ω_B	dimensionless betatron frequency
ω_0	undulator frequency
D	dose
E_c	critical energy
e^-	electron
e^+	positron
H	dose rate
P_{TSP}	total stopping power
R_{CSDA}	continuous stopping distance approximation range
X_0	radiation length
Z	atomic number

LIST OF ACRONYMS

CFR	Code of Federal Regulations
DOE	Department of Energy
FEL	Free Electron Laser
GDR	Giant Dipole Resonance
LINAC	Linear Accelerator
NPS	Naval Postgraduate School
NRC	Nuclear Regulatory Commission
RF	Radiofrequency
TLD	Thermo Luminescent Dosimeter

THIS PAGE INTENTIONALLY LEFT BLANK

ACKNOWLEDGMENTS

I would like to first thank Professor Colson for his time and insight through this amazing journey. His ability to help me understand this material was instrumental in me completing this thesis. I would also like to thank Professor Cohn for his slugging it out in the trenches with me learning these simulation programs. His patience and sense of humor helped especially when it seemed like our research was not going anywhere. I would also like to thank the rest of the FEL group for the entertaining time at NPS. Only in the Navy can you bring together such a wide range of interesting characters.

This process whole process would not have been possible without my family's support. It has been a long two years being away and missing time with my family. My boys, Mark and Reid, have grown so much and I could not have asked for better sons. My wife, Nanette, has been a single parent through all this and has done an amazing job! I look forward to coming home and trying to catch up on all the time missed.

Lastly, I would like to thank my Dad and Grandfather. Even though I lost both of them during this time here at school, their encouraging words helped when school seemed overwhelming. So I say here's to you, Dad and Grandpa. SEMPER FI!!!

THIS PAGE INTENTIONALLY LEFT BLANK

I. INTRODUCTION

A. HISTORY

The Light Amplification by Stimulated Emission of Radiation (laser) can be traced back almost 100 years. Albert Einstein first proposed the theory of stimulated emissions in 1917. Then by World War II, the development of radar and other components allowed the coherent microwave radiation to be produced. Components of these radar systems, such as traveling-wave tubes, magnetrons, microwave tubes, and kylstrons, all would have an impact on the future development of lasers. The next step toward the laser was the variation called the maser ("Microwave Amplification by Stimulated Emission of Radiation") that was produced by Charles Townes and Arthur Schawlow in 1958 [1].

In 1960, Theodore Maiman was the first to show a working laser. The laser required an energy absorbing material, in this case a synthetic ruby crystal, and a flash lamp used as an excitation source [1]. Creation of the photon beam is accomplished by using the excitation source to pump energy into the absorbing material. Atoms in the material that were originally in the ground state are excited and raised to a higher energy state. The excited atoms transition to a lower energy state emitting a photon in the process. The photons released stimulate other atoms in the material, creating a cascade of photons. The photons are then collected in a cavity that uses optical lenses and mirrors to direct and focus the photon beam. Gordon Gould, who was a graduate student under Charles Townes, first created the term "laser." By 1970, a Russian scientist named Zhores Alferov and an American scientist, Morton Panish, developed a diode laser that was able to operate continuously at room temperature [1].

J.M.J. Madey proposed the first Free Electron Laser (FEL) in 1971 at Stanford University [2]. His approach to the laser was to use a combination of different concepts, building on the work of Motz, Phillips and others. Madey used undulators, optical resonators, and application of concepts from microwave tubes with atomic lasers.

Microwave tubes are tunable and have a good efficiency. Using a relativistic electron beam from a particle accelerator allowed for the added benefit of shorter wavelengths.

B. RESEARCH

Understanding the history of the laser shows the importance and rate in which they are developing. As FELs become more powerful, they have opportunities ranging from commercial applications to scientific research. Even space applications of the FEL hold a lot of promise [3]. This is due to the fact that FELs are tunable and becoming more powerful, so they might overcome some of the challenges that atmospheric conditions present. As the power of these FELs increases, the radiological hazards also increase. This thesis will look at a hypothetical FEL and assess some of the radiological concerns. The area of focus will be on specific electrons that may generate radiation and how to relate it to shielding requirements. Different shielding configurations will be analyzed to look at the possibility of shielding a compact FEL.

The thesis will cover, in Chapters II and III, the physical construction of a FEL and the purpose of the components. The chapters will also discuss the theory of operation and how the FEL creates a useable laser beam.

Chapter IV will discuss what halo electrons are and possible generation sources. This chapter will also cover halo electron transport and concerns with the interception of halo electron by beam line components.

Chapter V and VI will discuss radiation production theory and what radiation is produced from electrons colliding with beam line materials. The radiation limits associated with operating the FEL and the computer program used to evaluate the radiation shielding will be discussed.

Chapter VII will present several types of shielding models that could be used for this notional FEL. This chapter will discuss benefits of using the different models and show their effectiveness.

II. FREE ELECTRON LASER DESCRIPTION

An FEL generates electromagnetic radiation from a relativistic beam of electrons. Two basic design configurations are the oscillator and the amplifier designs. Both designs have many of the same components. An amplifier design amplifies an existing "seed" optical field and relies on the electron beam energy being transferred to the light wave on a single pass through the undulator. The oscillator is designed with an optical cavity that is enclosed by mirrors and contains an undulator in the middle. A small percentage of electron energy is transferred to the optical beam in both designs. Figure 1 shows a diagram of a recirculating energy recovery FEL.

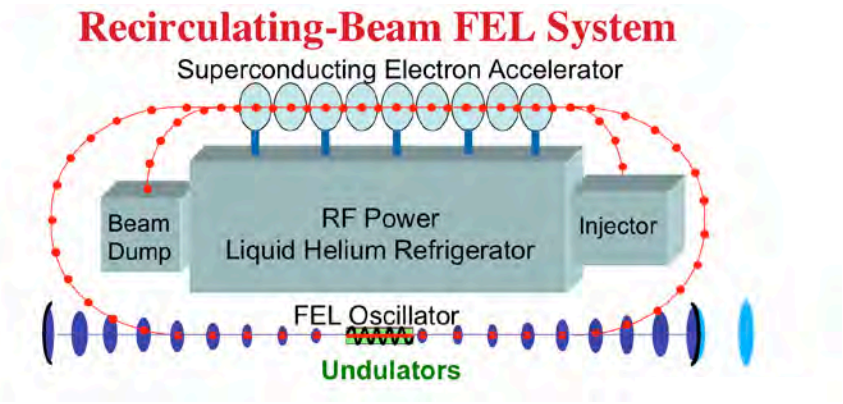

Figure 1. FEL schematic [After 3]

A. FEL COMPONENTS

Some of the major components of the FEL are the injector, accelerator, undulator, resonator (oscillator design), seed laser (amplifier design), and beam dump. Other components used to shape and direct the electron beam are the focusing/bending magnets and beam piping.

1. Injector

The creation of the electron beam begins with the injector. Two key components of the injector are the electron gun and cathode. Cathodes can produce electrons in a few different methods.

a. Field Emission Cathodes

Field emission cathodes use high electric fields from sharpened metal tips to generate the free electrons.

b. Thermionic cathodes

These cathodes use heat to "boil" electrons off of a metal surface. Heating of metal adds thermal energy in the metal and allows the energy deposited to exceed the work function, thereby freeing electrons.

c. Photocathodes

These cathodes release electrons using the photoelectric effect with a pulsed drive laser of appropriate pulse length and energy (Figure 2). Based on the cathode material, the drive laser wavelength used will be chosen to overcome the work function for the material. The drive laser also determines the electron pulse structure.

The two primary types of electron guns are direct current (DC) and radiofrequency (RF). Direct current electron guns can be limited by an acceleration gradient of less than 6 MV/m. This can limit the charge per bunch of the electron pulses to less than 1 nC [5]. RF electron guns are capable of higher acceleration gradients and larger charge per bunch. In the injector, electrons from the cathode are released and emitted into an RF cavity. The electrons can be accelerated in the RF cavity to higher energies (~5MeV) prior to entering the linear accelerator.

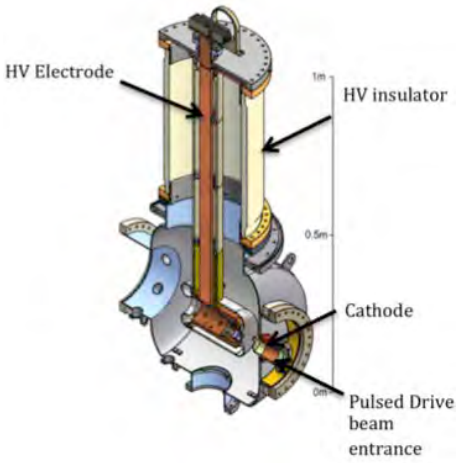

Figure 2. Photocathode injector layout with pulsed drive entering and creating the electron beam [After 6]

2. Linear Accelerator

Electrons produced from the injector are directed to the accelerator. The linear accelerator (LINAC) consists of several superconducting radiofrequency (SRF) cavities (Figure 3). These cavities can have acceleration gradients of ~18 MV/m [5]. The high voltage electromagnetic fields on axis are synchronized to the electron beam pulses. This allows for the electrons entering at 5 MeV to be accelerated up to relativistic energies of 100 MeV after passing through ~10 cavities [7].

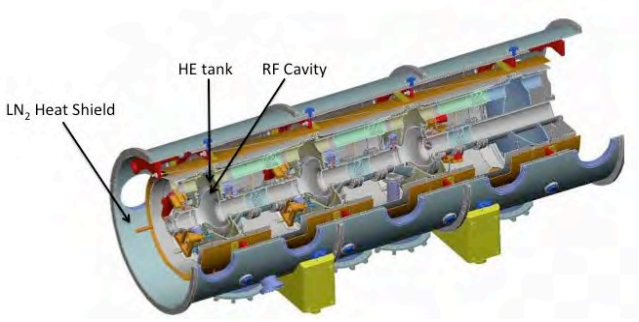

Figure 3. FEL accelerator cryomodule where electrons will enter through the center and be accelerated from ~5 MeV to 100 MeV [After 8]

3. Undulator

The electron beam leaving the accelerator will be directed into the undulator, in the middle of the optical cavity. The undulator consists of a series of permanent magnets that are configured to create an alternating magnetic field. As the electrons enter into the undulator they encounter a strong periodic magnetic field. The strong Lorenz forces move the electrons back and forth due to the alternating magnetic fields, causing the relativistic electrons to emit photons. The undulator length is typically much larger for an amplifier FEL in order to achieve the required high optical gain over a single pass. Undulators can have a helical or linear type design. Figure 4 shows a design of a linear undulator.

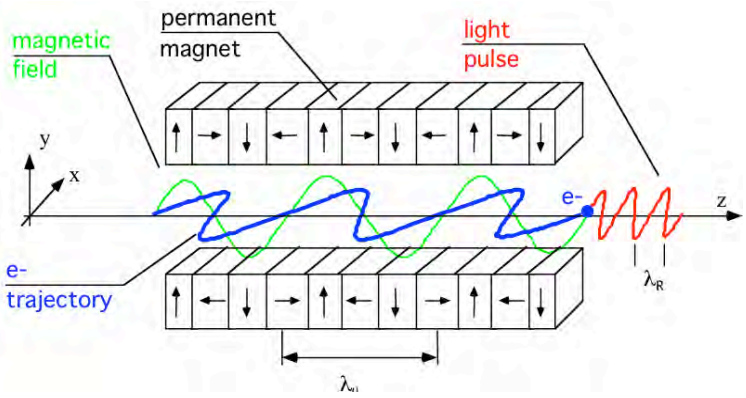

Figure 4. Schematic of linear undulator magnet orientation [From 9]

4. Optical Cavity

In an FEL oscillator the optical cavity, also called the resonator, contains two mirrors surrounding the undulator. A optical beam will travel down the undulator each pass and will hit a highly reflective mirror, then be redirected back through the undulator to another mirror that is partially transmissive. Reflection of the optical beam back through the undulator is timed with the electron beam pulses to ensure continual overlap over many passes. The partially transmissive mirror allows for a fractional amount of the optical beam to be transmitted to the beam director and out from the ship. It is important

to note that FEL designs can operate without the use of an optical cavity just described. Amplifier FELs use seed lasers in conjunction with the undulator to create the optical beam.

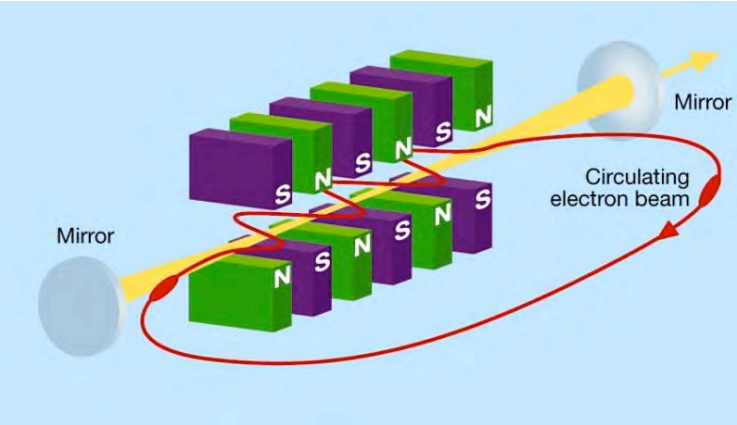

Figure 5. Optical cavity for oscillator FEL [From 10]

5. Beam Line Support Components

The electron beam after creation in the injector has to be continually manipulated in order to ensure it follows the desired path. Components used to achieve control of the electron beam in the beam piping are the bending magnets and focusing magnets. Bending magnets direct the electron beam for circulation, while focusing magnets direct the electron beam envelope along the propagation axis. A vacuum is maintained in the beam piping and components to reduce electron scattering with particles. The core electron beam traveling within the beam piping will have a diameter of ~1mm and the piping will have a diameter of ~5 cm. Not all electrons created will be contained within the core electron beam. Some electrons will exist between the beam pipe and the outside of the core beam as shown in Figure 6. These electrons are known as halo electrons. A fraction of the halo electrons will interact with beam line components as they travel along the FEL electron beam path. This particle interaction with the beam line components will result in the creation of radiation. Since this particle interaction is occurring at high energies (>7 MeV), more significant neutron and photon radiation will be produced.

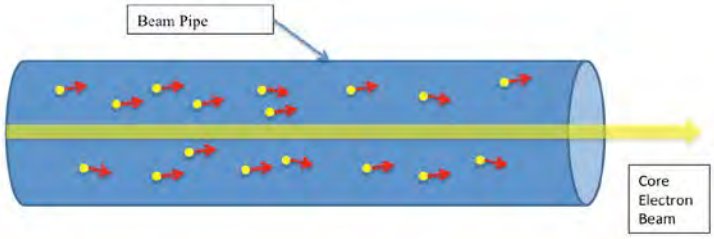

Figure 6. Halo Electrons outside core beam

6. Beam Dump

In an ERL FEL the electrons leave the optical cavity and then are redirected back through the LINAC using bending magnets. However, the electrons will enter the LINAC 180° out of phase with the RF. This will allow the electrons to release energy to the RF field as they are decelerated. This transfer of energy will lower the electrons from ~98 MeV down to ~5MeV [5]. After the electron beam leaves the LINAC, it is absorbed by the beam dump. The beam dump consists of a large block of absorbing material, such as copper, and enclosed with shielding. Shielding is required due to the energy of the electrons being absorbed and radiation being produced. Another outcome of this absorption is thermal heating, and this requires the beam dump to be cooled. Dumping the electron beam at less than ~10 MeV has the advantage of not producing neutrons. So that shielding needs are greatly reduced and lowers activation concerns. A majority of the halo electrons that are produced in the FEL will travel through the beam line components and make it to the beam dump with the core electron beam.

III. BASIC FEL THEORY

The aspect of how and why the FEL operates is best understood by knowing how the electrons behave within the undulator in the presence of light. A mathematical description of the electron motion through the undulator will allow for this understanding and also provide insight in a halo electron's fate during the operation of the FEL.

A. THE PENDULUM EQUATION

Electrons created in the injector will be traveling at high energies and relativistic speeds upon leaving the accelerator. The focus of this section will be on the electron beam motion inside the undulator. This is a critical component of the FEL that provides for the interaction between the electrons and the photons.

Electrons in the undulator will experience interactions with both the optical and undulator fields. These dynamic electron interactions will be examined by treating them classically. This due to the free electrons in the FEL not being constrained by the quantum mechanics of electrons in lasing materials in other laser designs. This classical treatment of the electrons allows for the correlation of the microscopic motion of the electrons to the equation of motion of the classical pendulum.

To understand this correlation, we must first understand the relationship between the electrons and photons. Photons will be traveling through the undulator at the speed of light, c. Electrons will be traveling down the undulator at a slightly slow speed, according to $z(t) = \beta_z ct$, where $\beta_z = v_z / c$ and v_z is longitudinal speed of the electron. Figure 6 shows this relationship between electrons and photons as a race where λ_o is the undulator wavelength and λ is the optical wavelength.

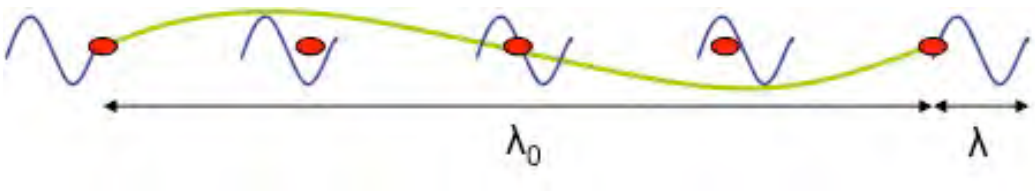

Figure 7. Electron-Photon interaction [From 7]

As photons and electrons travel down the undulator, photons will overtake the electrons. As the electrons travel down the undulator they will interact with the magnetic field. The magnetic field in the helical undulator on axis can be represented by

$$\vec{B}_u = B(\cos(k_o z), \sin(k_o z), 0), \tag{1}$$

where $k_o = 2\pi / \lambda_o$ is the undulator wavenumber. The difference in the photon's and electron's velocity along the undulator axis is given by [4]

$$c - v_z = c - c\beta_z, \tag{2}$$

where $\beta_z \approx 1 - (1 + K^2)/(2\gamma^2)$ using $\gamma^{-2} = 1 - \beta_\perp^2 - \beta_z^2$, $\gamma \gg 1$ is Lorentz factor, $K = eB\lambda_0 / (2\pi mc^2)$ is the undulator parameter, m is the mass of an electron, and $e = |e|$ is electron charge magnitude, and $\beta_\perp$ is the transverse velocity.

The optical field consists of an electric field and a magnetic field (cgs units)

$$\vec{E}_0 = E(\cos\psi, -\sin\psi, 0), \tag{3}$$

$$\vec{B}_0 = E(\sin\psi, \cos\psi, 0), \tag{4}$$

where E is the electric field amplitude, $k = 2\pi / \lambda$ is the wave number, λ is the wavelength, and $\psi = kz - \omega t + \phi$. The net electron motion in all fields in the undulator can be represented by the relativistic Lorenz force equations

$$\frac{d(\gamma\vec{\beta})}{dt} = -\frac{e}{mc}(\vec{E} + \vec{\beta} \times \vec{B}), \tag{5}$$

$$\frac{d\gamma}{dt} = -\frac{e}{mc}\vec{\beta} \cdot \vec{E}, \tag{6}$$

where $\vec{v} = c\vec{\beta}$ is the electron velocity. The optical and undulator fields (1), (3), and (4) can be inserted into (5) and (6) to give [7]

$$\frac{d(\gamma\beta_z)}{dt} = -\frac{e}{mc}\left[E(\beta_x \cos\psi - \beta_y \sin\psi) + B(\beta_x \sin k_o z - \beta_y \cos k_0 z)\right], \tag{7}$$

$$\frac{d(\gamma\vec{\beta}_\perp)}{dt} = -\frac{e}{mc}\left[E(1 - \beta_z)(\cos\psi, -\sin\psi, 0) + \beta_z B(-\sin k_0 z, \cos k_0 z, 0)\right], \tag{8}$$

$$\frac{d\gamma}{dt} = -\frac{e}{mc}E\left[\beta_x \cos\psi - \beta_y \sin\psi\right], \tag{9}$$

where $\vec{\beta}_\perp = \beta_x \hat{i} + \beta_y \hat{j}$. Relativistic electrons will be assumed as traveling at approximately the speed of light c, so that $\beta_z \approx 1$. This allows for integration of (8) knowing that $B\beta_z \gg E(1-\beta_z)$ so that the result can be represented as [4]

$$\vec{\beta}_\perp = -\frac{K}{\gamma}(\cos k_0 z, \sin k_0 z, 0). \tag{10}$$

Therefore, $\beta_\perp^2 = \frac{K^2}{\gamma^2}$ and K represents the dimensionless undulator parameter. The transverse motion through the undulator (10) was assumed to have the electrons injected perfectly into helical orbits, so the constant of integration is zero.

The distance that one photon gets ahead of the electron in distance λ_0 and in a time λ_0 / β_z determines the resonant wavelength, λ. The value for λ is then [7]

$$\lambda = (1-\beta_z)\lambda_0 / \beta_z \approx \lambda_0 (1+K^2)/2\gamma^2. \tag{11}$$

This is the resonance condition when one wavelength of light passes over an electron in one undulator wavelength.

The microscopic motion of the electrons can now be solved by substituting (10) into (9) and gives

$$\dot{\gamma} = \frac{eKE}{\gamma mc}\cos(\varsigma + \phi) \tag{12}$$

,

where ς is the electron phase, $\varsigma(t) = (k + k_o)z - \omega t$. For relativistic electrons $k \gg k_o$ and $\lambda \gg \lambda_o$. The electron phase at $t = 0$ is $\varsigma(0) = (k + k_o)z_o$, where z_o is the initial position of the electron.

Continuing to solve for the pendulum equation we now substitute (10) into $\gamma^{-2} = 1 - \beta_\perp^2 - \beta_z^2$ which results in [7]

$$\gamma^{-2} = 1 - \beta_z^2 - \beta_\perp^2 = 1 - \beta_z^2 - K^2/\gamma^2 \Rightarrow 1 - \beta_z^2 = (1+K^2)\gamma^{-2}. \tag{13}$$

Taking the time derivative of (13) establishes the relationship between $d\beta/dt$ and $d\gamma/dt$ as

$$\frac{\dot{\gamma}}{\gamma} = \frac{\gamma^2 \beta_z \dot{\beta}_z}{(1+K^2)}. \tag{14}$$

Taking the second time derivative of $\varsigma(t) = (k + k_o)z - \omega t$ gives

$$\ddot{\varsigma} = (k + k_o)c\dot{\beta}_z. \tag{15}$$

Now we can take (15) and substitute it into (14) and remembering that for relativistic electrons $k \gg k_o$ since $\beta_z \approx 1$ and $\gamma \gg 1$. The result is

$$\frac{\dot{\gamma}}{\gamma} = \frac{\gamma^2 \ddot{\varsigma}}{\omega(1+K^2)}. \tag{16}$$

The resonance condition stated from (3) and microscopic electron motion from (12) can be substituted into (16) to give,

$$\ddot{\varsigma} = \frac{2\omega_o eKE}{\gamma^2 mc}\cos(\varsigma + \phi). \tag{17}$$

For ease of understanding the FEL operation, the next step is create a dimensionless parameter for time, τ. This dimensionless time parameter is $\tau = ct/L$, where L is the length of the undulator. Another dimensionless parameter is $|a| = 4\pi NeKLE/(\gamma^2 mc^2)$ that represents the optical field amplitude. Indications of strong or weak optical fields are related to the value of the optical field amplitude, $|a|$; if $|a| \ll \pi$, the optical field is weak and core electrons only move the electron phase by $\ll \pi$. If $|a| \gtrsim \pi$, the optical fields are strong since the electron phase maybe changed by $\sim \pi$, changing the sign of energy exchange.

The electron phase velocity represents the rate of change of the electron phase as it transits down the undulator ($\tau = 0 \to 1$) and the equation is

$$v = \dot{\varsigma} = \varsigma' L/c \tag{18}$$

where $\dot{(...)} = d(...)/d\tau$. These parameters are used to simplify (17) to

$$\ddot{\varsigma} = |a|\cos(\varsigma + \phi) \tag{19}$$

which represents the of microscopic electron motion in the form of the pendulum equation.

B. OPTICAL WAVE EQUATION

In the previous section we derived the microscopic motion of an electron through the undulator. As the electrons travel through the undulator, their wiggling motion will generate and amplify light. These photons will create an optical field that will interact with the source current of the bunching electrons traveling through the undulator. We will now develop the wave equation describing the evolution of light.

Starting from Maxwell's equations, the wave equation can be written in cgs units as [11]

$$\left(\nabla^2 - \frac{\partial^2}{\partial t^2 / c^2} \right) \vec{A}(\vec{x},t) = -\frac{4\pi}{c} \vec{J}_\perp(\vec{x},t), \tag{20}$$

where $\nabla = \hat{i}\,\partial/\partial x + \hat{j}\,\partial/\partial y + \hat{k}\,\partial/\partial z$, $\vec{A}$ is the optical potential vector, and $\vec{J}_\perp$ is the electron current. The optical potential vector gives the electric and magnetic fields of the laser. In order to create a basic equation for the optical potential vector we can consider that the coherent laser field changes slowly over time compare to the optical frequency. The optical potential vector for the helical undulator is written as [11]

$$\vec{A}(\vec{x},t) = \frac{E(\vec{x},t)}{k} \hat{\varepsilon} e^{i\alpha} \tag{21}$$

where the polarization vector of the helical undulator is $\varepsilon = (-i, 1, 0)$, $\alpha = kz - \omega t$ is the phase of the carrier wave, and E is the laser's complex electric field. The simplified optical potential vector is inserted into (20). The field, $E = |E| e^{i\phi}$, is assumed to vary slowly in time during the optical period $\left(\dot{E} \ll kE, \phi' \ll \omega\phi \right)$, and slowly in space over an optical wavelength $\left(E' \ll kE, \phi' \ll k\phi \right)$ where ($'$) represents differentiation with respect to z. [11] These assumptions allow the general wave equation to be represented as the parabolic or paraxial wave equation, [4]

$$\left[\nabla_\perp^2 + 2ik\left(\frac{1}{c}\frac{\partial}{\partial t} \right) \right] E = -\frac{4\pi k}{c} \vec{J}_\perp \cdot \hat{\varepsilon}^* e^{-i\alpha}, \tag{22}$$

with $\vec{J}_\perp$ representing the total beam transverse current and $\nabla_\perp^2$ represents the transverse Laplacian containing the partial derivatives in both the x and y coordinates. The total beam current represents the summation of all the single-particle currents and is given by

$$\vec{J}_\perp = ec\sum_i \vec{\beta}_\perp \delta^{(3)}\left(\vec{x} - \vec{r}_i(t)\right), \tag{23}$$

where $\vec{r}_i(t)$ is the trajectory of the *i*th electron, $\vec{\beta}_\perp$ is electron's transverse motion, and $\delta^{(3)}$ is the 3-dimensional Dirac delta function.

Recall that the transverse electron motion is

$$\vec{\beta}_\perp = -\frac{K}{\gamma}(\cos k_0 z, \sin k_0 z, 0) = \mathrm{Re}\left(-\frac{K}{\gamma} i\hat{\varepsilon} e^{-ik_0 z}\right), \tag{24}$$

where $\mathrm{Re}()$ indicates taking the real part. The transverse electron motion (24) can be inserted into (23) and the result can be used in the parabolic wave equation (22). The results from this substitution are

$$\left[-\frac{iL}{2k}\nabla_\perp^2 + \frac{\partial}{\partial\tau}\right] a(\vec{x},\tau) = -\left\langle je^{-i\varsigma}\right\rangle_{(\vec{x},\tau)}, \tag{25}$$

where $j = 8\pi^2 Ne^2K^2L^2\rho/\gamma_0^3 mc^2$ is the dimensionless FEL current density, $|a| = 4\pi NeKL|E|/\gamma_0^2 mc^2$ is the dimensionless laser field, < > represents the average over the electrons in the beam, and ρ is the electron particle density.

Further simplification of (25) can be achieved by creating a dimensionless Laplacian operator. The introduction of natural dimensionless transverse coordinates $\tilde{x} = x(k/2L)^{1/2}$ and $\tilde{y} = y(k/2L)^{1/2}$ allows for the new Laplacian to be represented by $\tilde{\nabla}_\perp^2 = \partial_{\tilde{x}}^2 + \partial_{\tilde{y}}^2$. The dimensionless wave equation can now be written as [11]

$$\left[-\frac{i}{4}\tilde{\nabla}_\perp^2 + \frac{\partial}{\partial\tau}\right] a(\vec{r},\tau) = -\left\langle je^{-i\varsigma}\right\rangle. \tag{26}$$

Diffraction of the beam is described by the left side of (26). When conditions of small diffraction exist, the $\nabla_\perp^2$ term is negligible small so that (26) can be simplified to

$$\overset{\circ}{a} = -j\left\langle e^{-i\varsigma}\right\rangle. \tag{27}$$

The amount of electron bunching is represented in (31) by the average $\langle e^{-i\varsigma} \rangle$, and the measure of the coupling between the optical and electron beams is represented by the dimensionless current density, j. Both the average electron phase and the dimensionless current have an effect on the rate of change in the optical field. If $j < \pi$, there will be only a small coupling between the beams, and with $j \ll \pi$, large coupling is present.

C. OPTICAL GAIN

Optical gain is the fractional gain of the optical beam power or energy and can be determined by the total energy lost by the electron beam. Interactions between the electrons and the optical beam allow for energy transfer to occur. The two equations that allow us to understand that interactions between electrons and photons are

$$\dot{a} = -j\langle e^{-i\varsigma} \rangle, \quad \ddot{\varsigma} = |a| \cos(\varsigma + \phi).$$

As previously stated $|a|$ is the dimensionless optical amplitude and determines whether the FEL is operating in strong or weak fields. If $|a| < \pi$, the optical field is weak, and if $|a| > \pi$, the optical field is strong. The optical phase is ϕ.

The amplitude and phase evolution can be estimated in the case of weak fields $(a_0 \ll \pi)$ and low gain $j < \pi$ $(|a| \ll a_0)$. Then, using the power series expansion for ς, (27) can solved for the lowest order change in the field and phase [11] yielding

$$|a(\tau)| = a_0 \left(1 + j \left(\frac{2 - 2\cos(\upsilon_0 \tau) - \upsilon_0 \tau \sin(\upsilon_0 \tau)}{2\upsilon_0^3} \right) \right) + \ldots, \text{ and} \tag{28}$$

$$\phi(\tau) = j \left(\frac{2\sin(\upsilon_0 \tau) - \upsilon_0 \tau (1 + \cos(\upsilon_0 \tau))}{2\upsilon_0^3} \right) + \ldots \tag{29}$$

where ν_0 is the initial phase velocity of the electron beam. In this region, the gain is

$$G(\tau) = j \left(\frac{2 - \cos(\upsilon_0 \tau) - \upsilon_0 \tau \sin(\upsilon_0 \tau)}{\upsilon_0^3} \right). \tag{30}$$

The gain can also be estimated for $j \ll \pi$ and weak fields. In this regime, (28)-(30) changes to the following

$$|a(\tau)| \approx \tfrac{1}{3} a_0 \exp\left[\left(\tfrac{1}{2} j\right)^{1/3} \sqrt{3}\left(\tfrac{1}{2}\right)\tau\right], \tag{31}$$

$$\phi(\tau) \approx \left(\tfrac{1}{2} j\right)^{1/3} \tfrac{1}{2}\tau, \text{ and} \tag{32}$$

$$G(\tau) \approx \tfrac{1}{9} \exp\left[\left(\tfrac{j}{2}\right)^{1/3} \sqrt{3}\tau\right]. \tag{33}$$

In general, simulations must solve the electron pendulum and optical wave equations self-consistently.

In Figure 8, it is shown that at resonance $(\upsilon_0 = 0)$ that there is electron bunching, but gain with phase velocity slightly off-resonance ($\upsilon_0 = 3$) can be significantly larger as shown in Figure 9. The thin upper and lower boundary in Figures 8 – 10 is the separatrix. The thin traces from yellow to blue dot represent the electron's initial and final positions within phase space. Change in the vertical axis (υ) can be related to the change in electron energy $\Delta\upsilon = 4\pi N \dfrac{\Delta\gamma}{\gamma}$, where $\dfrac{\Delta\gamma}{\gamma}$ represents the change in energy.

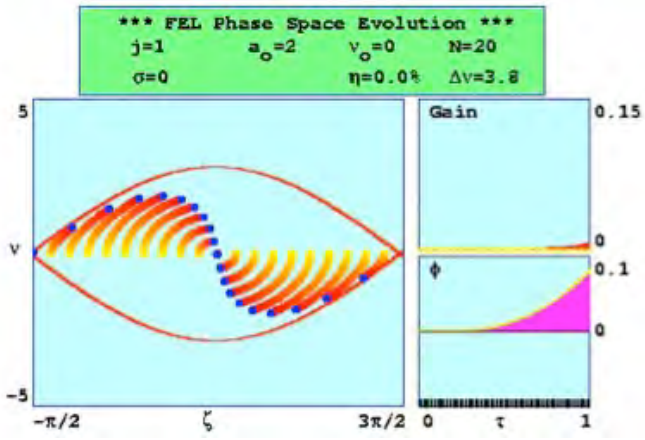

Figure 8. Electron phase velocity at resonance [From 4]

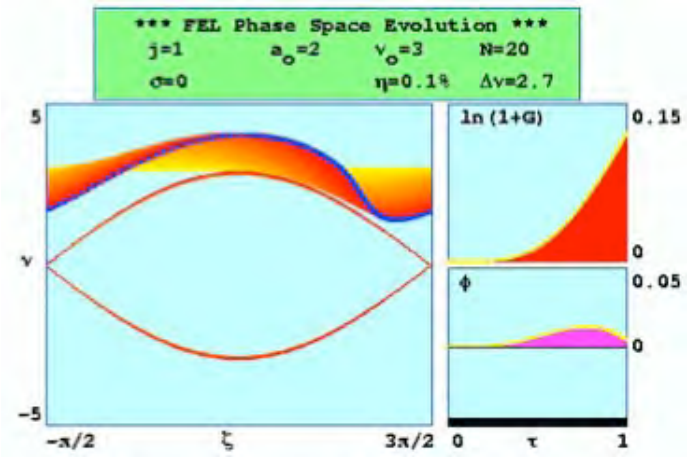

Figure 9. Electron phase velocity off-resonance [From 4]

For strong fields, $|a| = 20 \gtrsim \pi$, over-bunching of the electrons can occur. This over-bunching causes electrons to shift from the proper phase for gain to one for absorption, as seen in the Figure 10. As a result, the gain decreases significantly.

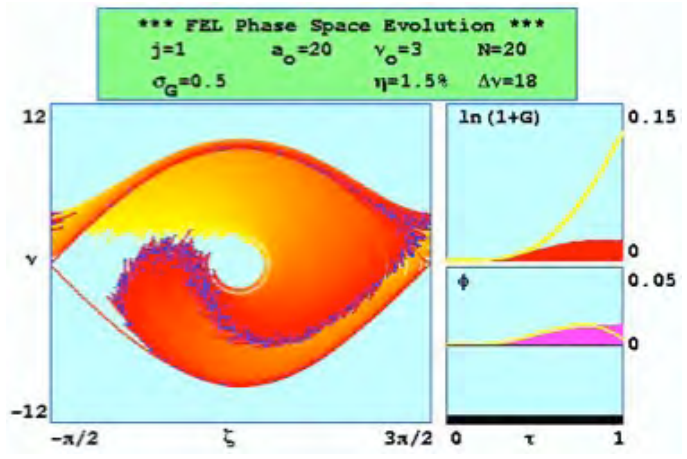

Figure 10. Strong optical fields ($|a| \gtrsim \pi$) [From 4]

THIS PAGE INTENTIONALLY LEFT BLANK

IV. HALO ELECTRONS

Halo electrons are the electrons that exist outside the core electron beam. The halo electrons can travel all the way to the beam dump located at the end of the electron beam path. But, some halo electrons do not make it to the beam dump, and can produce significant amount of radiation that is hazardous to both personnel and equipment. This chapter will briefly discuss the potential sources of halo electrons and their transport through some beam line components.

A. HALO GENERATION

The generation of halo electrons can be from several possible sources. All of the mechanisms that generate these electrons are not fully understood. Generally, halo electrons are those electrons outside the core of the electron beam. The distance that halo electrons are from the core electron beam can vary from a few rms beam radii to approximately 10 rms beam radii [12].

One of the potential sources for halo electrons is the scattering of drive laser light at the injector cathode. The surface quality of the cathode can also contribute to the amount of scattering, especially in the area near the edge of the emitter, and can be a significant contributor to the generation of halo electrons [13].

B. HALO TRANSPORT

Other possible sources of halo electrons are from transport of the electrons. Transport of the halo electrons depends on the position and angle of the electrons within the beamline. Together these parameters define the phase space of the electrons during the transport through the FEL components. The radius, r_b, in phase space is the distance of one electron from the center of the beamline. Each electron also has an angle, θ_b, with respect to the beamline axis. Figure 11 shows how the halo electrons can exist outside of the core electron beam in phase space.

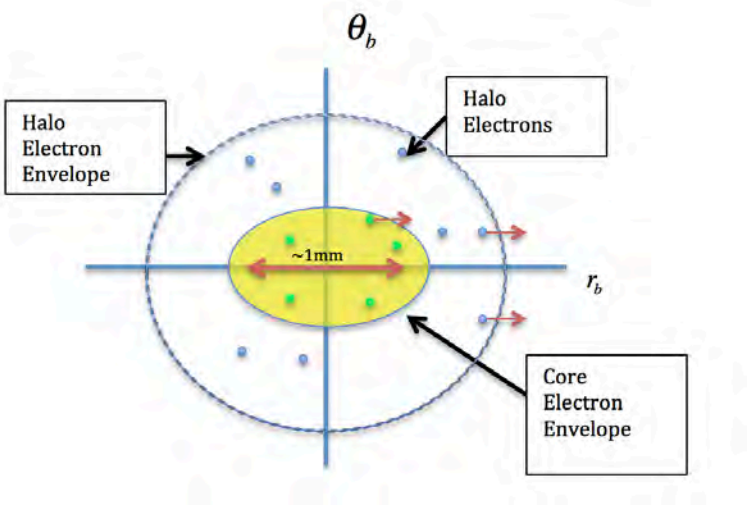

Figure 11. Core and halo electron beam phase space

The envelope of electron positions and angles can be related to the normalized transverse emittance parameter, given by [4]

$$\varepsilon_n = \gamma r_b \theta_b, \tag{34}$$

where γ is the Lorentz factor, r_b is the core rms electron beam radius, and θ_b is the rms electron beam angle. A typical value of emittance is $\varepsilon_n \approx 10$ mm-mrad, and a typical value for the electron beam Lorentz factor is $\gamma \approx 200$ (≈ 100 MeV). For a beam with an rms radius of 0.5 mm, the resulting angular spread is then $\theta_b \approx 0.1$mrad. The amount of halo electrons that collide with inner surfaces of the beamline components over some distance are dependent on both radial position and angle of a halo electron.

Assume a drift distance between components in the beam of $\Delta z \approx 1$m. The typical amount that electrons drift during the distance Δz is

$$\Delta r_b \sim \theta_b \Delta z \approx 0.1\text{mm}. \tag{35}$$

This shows that electrons inside the core electron beam will generally stay in the core since $\Delta r_b \sim 0.1$mm $\ll r_\phi \approx 1$mm. Halo electrons outside the core may not travel $\sim$1m before hitting the beam pipe, because a combination of their radial position and angular drift exceeds the beam pipe radius, $r_p \sim 5$cm.

Bending magnets can also have a contribution to the halo population. If the entering electron energy is outside the design envelop for the bending magnet, it may change the direction of those electrons by giving them excessive angles. These effects could also take a halo electron and collide it with the inner surface of the beamline.

Both bending and focusing magnets are intended to keep the electrons within the beam piping. Focusing magnets are also used to focus the electron beam to a smaller radius prior to entering the undulator. The electron beam will contain both the halo and core electrons. Once the electrons enter into the undulator they experience both fast oscillations and slow betatron motion as shown previously in Figure 4. This motion can be represented in the y-direction by [14]

$$y(\tau) = y_0 \cos(\omega_\beta \tau) + \frac{L\theta_y}{\omega_\beta} \sin(\omega_\beta \tau) \tag{36}$$

where y_o is the initial electron position, θ_y is initial electron angle, and $\tau = 0 \to 1$ is the dimensionless time parameter. The dimensionless betatron frequency is given by

$$\omega_\beta = \frac{2\pi NK}{\gamma}, \tag{37}$$

where N is the number of undulator periods and K is the dimensionless undulator parameter. Using (36) and (37) with $K \approx 1$, $\gamma = 200$, and $N = 20$ we can evaluate acceptable radial distances and angles for halo electrons in an undulator with a beam pipe having an inside diameter of 1 cm. If the electrons entering in the undulator have an excessive radial distance or angle, the electron will collide with the beam pipe. Figure 12 shows the approximate range of radial distances and angles that will transit through the undulator without collisions. A halo electron can make it through the narrowest part of the beamline, the undulator, if the electron enters with an acceptable radial distance and angle. In Figure 13, an amplifier undulator with 200 periods (x10 longer) is analyzed. The graph shows that with an increasing number of periods, the acceptable phase space is significantly smaller.

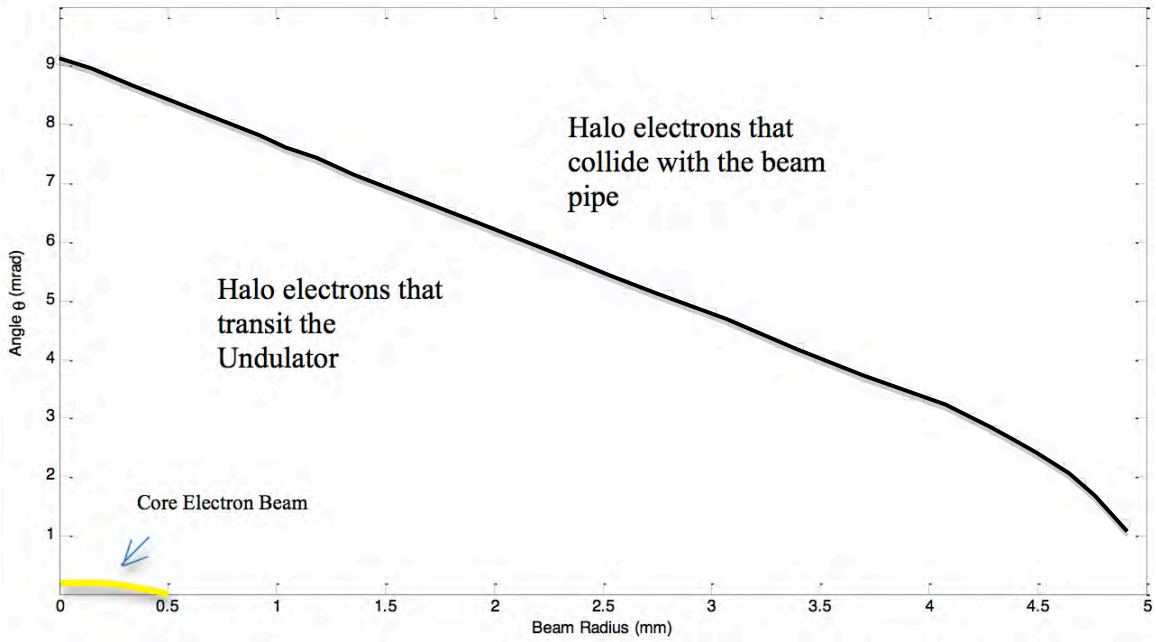

Figure 12. Acceptable angles and radial distance of electrons entering undulator (N=20)

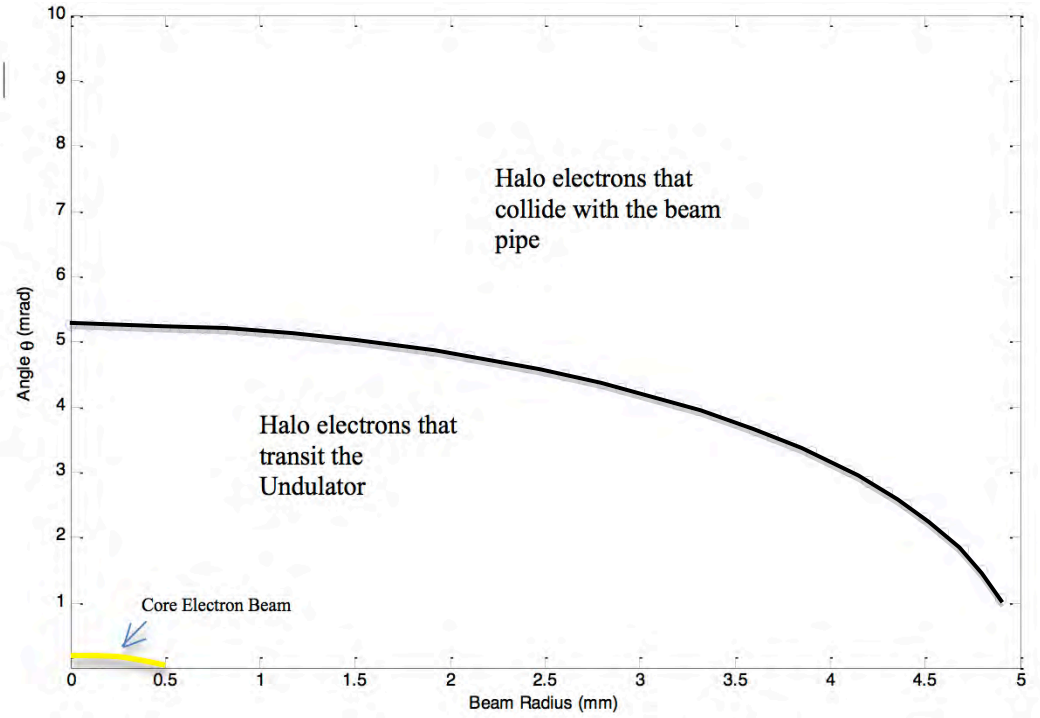

Figure 13. Acceptable angles and radial distance of electrons entering undulator (N=200)

V. RADIATION PRODUCTION AND SHIELDING

This chapter will provide a brief overview of particle interactions with matter. Some halo electrons described in the previous chapter can collide with various component materials as most of the electrons travel down the beamline. When these collisions occur the electrons lose their energy in the form of radiation. The initial energies of the electrons determine the types of interactions with the material and also the types of particles that may be created.

A. RADIATION TERMINOLOGY

Understanding the terminology and principles of measurement for radiation protection is key to comprehending the units of measurement and of the quantities obtained. High energy electrons interacting with matter can cause ionizing events to occur. When ionizations occur, there is some amount of energy being deposited in the material. A unit of measurement of this energy deposition in a material is the rad (1 rad = 0.01 J/Kg). This unit of measurement is referred to as an absorbed dose.

The unit of measurement of energy deposited in soft tissue should also account for biological effects. The amount of energy deposited in tissue is referred to as dose equivalent and the unit of measurement is the rem. There is significant scientific data that can relate dose equivalent to long and short-term health hazards, more information on this can be found on the EPA website. Both dose equivalent (rem) and absorbed dose (rad) refer to energy deposition and can be related to each other by the dimensionless quality factor Q, $rem = rad \times Q$ (see Table 1). The quality factor shows that for 1rad of neutron absorbed dose there will be 10 rem of neutron equivalent dose and 1 rad of gamma absorbed dose results in only 1 rem for gammas. This is due to the neutrons creating more ionizations within the soft tissue, which is related to biological damage.

Type of radiation	Quality factor (Q)	Absorbed dose equal to a unit dose equivalent[a]
X-ray, gamma, or beta radiation	1	1
Alpha particles, multiple-charged particles, fission fragments and heavy particles of unknown charge	20	0.05
Neutrons of unknown energy	10	0.1

Table 1. Typical Quality factor (Q) [After 15]

B. PHOTON PRODUCTION

The high-energy halo electrons (~100 MeV) that hit beamline components will lose energy either by radiative or collisional losses. Collisional losses occur through excitation and ionization processes. Radiative losses are associated with the creation of bremsstrahlung photons [16]. Energy loss (dE) per unit distance traveled (dx) for the electrons can be related to

$$\frac{dE}{dx} = \left(\frac{dE}{dx}\right)_{coll} + \left(\frac{dE}{dx}\right)_{rad}. \tag{38}$$

The collisional losses are primarily due to ionization and are a small portion of the total energy loss for high energy electrons. As the electron energy is lowered, the radiative losses for the higher energy electrons will become a smaller portion of the total energy lost and the collisional losses will become a larger portion of the total energy loss. The energy where collisional losses and the losses due to radiation (bremsstrahlung) are equal is called the critical energy, E_c. The critical energy is dependent on the type of material and can be given by [17]

$$E_c = \left(\frac{800 MeV}{Z + 1.2}\right), \tag{39}$$

where Z is the atomic number of the target material. When the electron energy is above the critical energy, the radiation losses will dominate, and when the electron energy is below the critical energy, the ionization losses are dominant.

Ionization is the process of either removing or adding charged particles from an atom. These charged particles are primarily electrons, but could include nucleons. The first ionization event between the incident particle and the atom will typically have the highest energy transfer. The average rate of energy losses due to ionization and excitation in relation to the average path an electron travels is called the collisional stopping power. Higher density materials have a larger impact on the collisional stopping power.

Radiation losses due to bremsstrahlung, "braking radiation," are the primary means of energy loss for high energy electrons. Bremsstrahlung is the process of the high energy electrons being deflected and decelerated by the nucleus of the atom in the target material. This change in direction and speed of the electron lowers the kinetic energy and emits a photon in this process due to electron acceleration (Figure 14). Relativistic electrons colliding with the target material will produce the highest concentration of photons in the general direction of the incident electron beam.

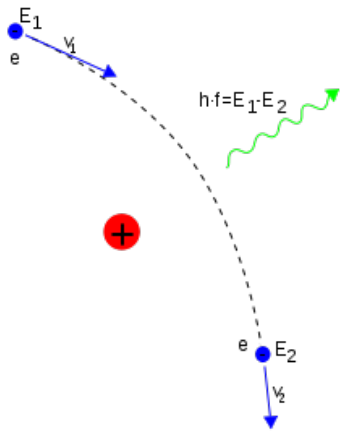

Figure 14. Bremsstrahlung process [From 18]

The average energy lost from the bremsstrahlung process over an average path traveled is called the "radiative stopping power." The sum of both the collision and radiative stopping powers is the "total stopping power." The total distance that the electron travels before it is stopped in the material is called the continuous stopping distance

approximation range (R_{CSDA}) [15]. The R_{CSDA} assumes that the electron entering into the material loses energy continuously over many atoms and can give an approximate penetration distance.

Another important distance parameter is the radiation length. The radiation length (X_0) describes the mean depth in the material in which the electron will have an energy reduction by a factor of e due to bremsstrahlung. Radiation length is affected by denser materials and as Z increases then X_0 decreases. When radiation losses are the primary mechanism of energy loss ($E_0 > E_c$), the electron energy at a certain depth is given by [17]

$$E = E_0 e^{-x/X_0}, \tag{40}$$

where x is the distance in the material and E_0 is the initial electron energy. Radiation length (X_0) can vary from ~37 cm for water to ~0.56 cm for lead. Figure 15 shows the percentage of photons produced when the electrons collide with various target materials. It is important to note that while higher Z materials have a lower E_c and therefore produce a larger amount of photons (Figure 15), they will also tend to have a shorter photon stopping distance. The remainder of the energy not converted to photons will be lost through ionization.

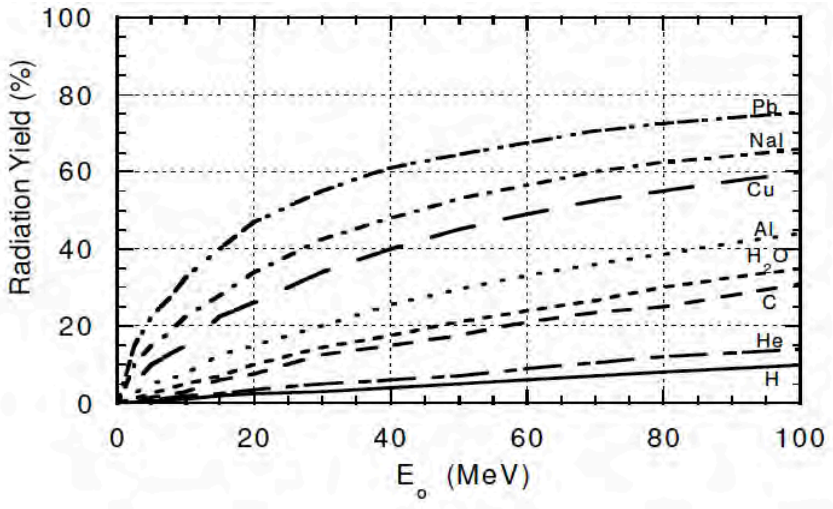

Figure 15. Percent yield of photons due to bremsstrahlung for various stopping materials for electrons [From 19]

C. NEUTRON PRODUCTION

Photons produced from bremsstrahlung can have various energies, depending on the initial energy of the electron. Photoneutron production generally begins when photon energies are at least 10 MeV. One of the main mechanisms of photoneutron production is the Giant Dipole Resonance (GDR). GDR produces neutrons when photons are incident on a target material and have an energy above the nuclear binding energy for the material (~7–30 MeV). The energy from the photon causes oscillations to occur within the nucleus and can result in a neutron being ejected. For lower energy electron beams (<100 MeV), GDR is the largest contributor of neutrons due to the large density of lower energy photons.

When the photon energies become greater (~30 to 300 MeV), the photoneutron production shifts to a Quasi Deuteron (QD) mechanism. This mechanism differs from the GDR in the way energy is imparted to the proton-neutron pair bonds. In contrast, GDR creates a resonance condition that causes neutron ejection [19].

D. ELECTROMAGNETIC CASCADE

An electromagnetic cascade will occur when the initial energy of an electron (E_0) is high enough to have radiative losses in the target material ($E_0 \gg E_c$). When the primary electron travels in the material a distance $\sim X_0$, typically a photon is produced. The energies of both the photon and electron at X_0 are typically $\sim E_0/2$. If the energy of the electron is high enough to continue to have radiative losses, it will travel another distance $\sim X_0$ before creating another photon. The photons produced will travel further in the material ($\sim 9/7\, X_0$) before it undergoes pair production and can create an electron-positron pair (e^+e^-) pair when photon energy is above 1.022 MeV. Energy of the e^+e^- pairs will be split ($\sim E_0/4$) from the photon undergoing pair production [17]. These e^+e^- pairs can continue and create photons again after traveling $\sim X_0$, resulting in a cascade as shown in Figure 16.

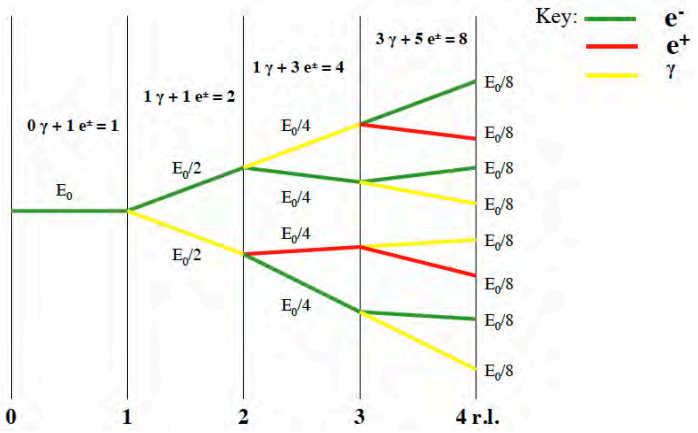

Figure 16. General overview of the electromagnetic cascade [From 20]

E. SHIELDING

Figure 17 shows dose equivalent values from both bremsstrahlung and photoneutrons when high energy electrons hit an unshielded target. The graph also shows how dose from bremsstrahlung has an angular dependency associated with the measured values.

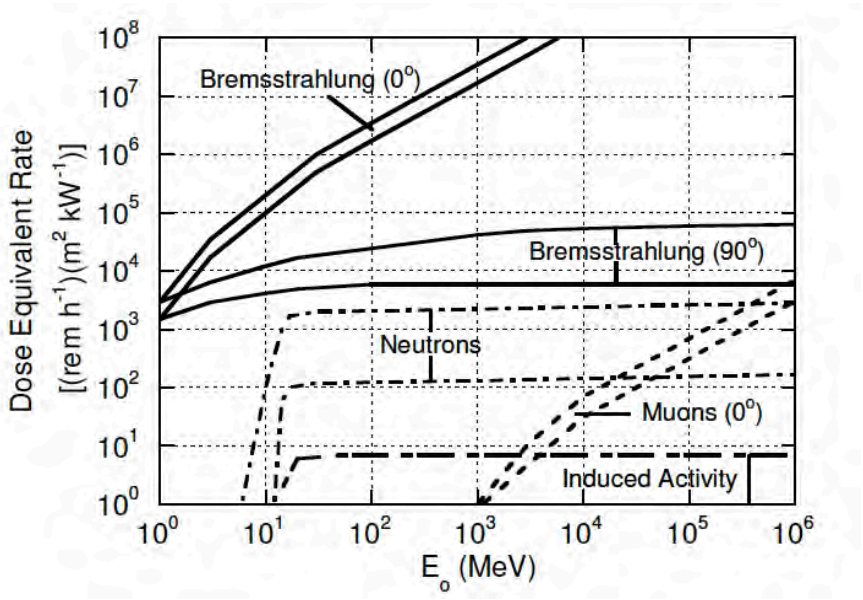

Figure 17. Dose equivalent from unshielded thick target material interaction with high energy electrons at 1 m [From 19]

The goal of a shielding design is to lower the energy of the radiation to a level that is safe for personnel and equipment. Many types of shielding materials are available for use and depend on the type of radiation that needs to be attenuated. Most shielding, if thick enough, will attenuate photon and neutron radiation. However, the design of the shielding should also take into account cost and size. In high energy electron cases, the photons produced are the primary radiation concern. This is due to the fact that the number of photons produced in the electromagnetic cascade is much higher than photoneutrons. Figure 18 shows the "half-value thicknesses" of materials for shielding against photons. The half-value thickness is the amount of material required to reduce the initial dose value by half. It is important to note that the higher the atomic number (Z) for a given material, the better the material attenuates photons, but the less effective it is in shielding neutrons. This is because a neutron transfers less of its kinetic energy in a collision with a heavier nucleus relative to a collision with a lighter nucleus. Shielding for neutrons is therefore most effective with materials containing high hydrogen content.

The dose through the shielding can be approximated by

$$H_{shielded} = \left(.5^{x/x_{1/2}}\right) H_{unshielded}, \tag{41}$$

where H is the photon dose rate (shielded and unshielded), x is the thickness of the material, and $x_{1/2}$ is the half-valued thickness. This equation will allow for hand calculations of shielding models in a later chapter to confirm simulation results. Multiple scattering events will lower the energy to the point where they will be absorbed into the material. It is important to note that when the neutrons are absorbed, the neutrons can release capture gammas. In most accelerator facilities, concrete is used as shielding for both photons and neutrons due to its high hydrogen content and relatively low cost, but this research will also explore the use of other materials.

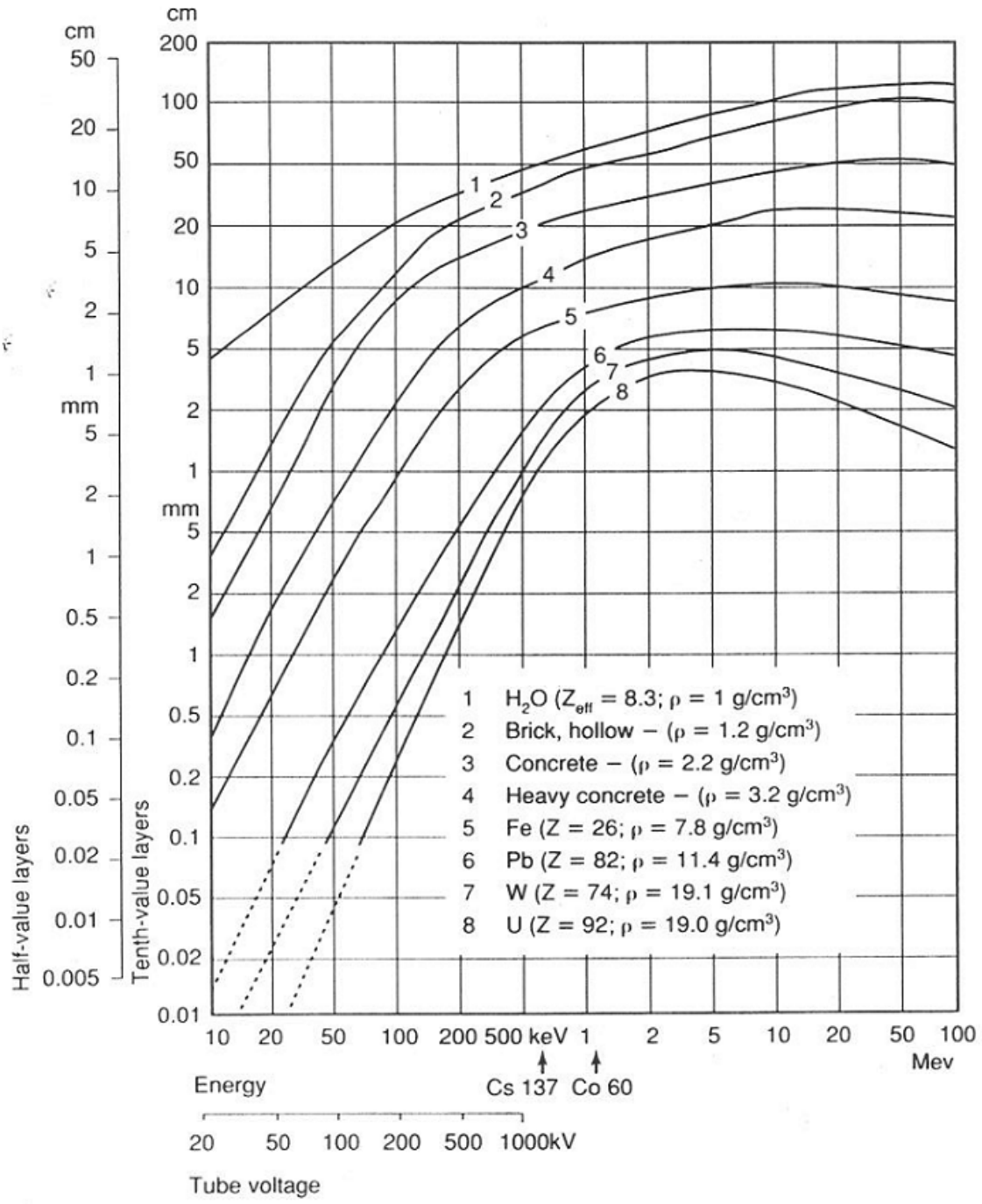

Figure 18. Half-Value layers for photons [From 21]

VI. EXPOSURE LIMITS AND MODELING SOFTWARE

A. EXPOSURE LIMITS

As discussed previously, radiation exposure from the operation of the ERL FEL can be a concern and is generally handled with the use of shielding. The establishment of acceptable radiation exposure determines the amount of shielding required for facility workers and the general public. Limits established by the Nuclear Regulatory Commission (NRC) are reported in document 10 CFR 20; those from the Department of Energy (DOE) are reported in 10 CFR 835. Both regulations have the same exposure limits for workers and the general public. The maximum annual exposure for workers is 5000 mrem/yr. The exposure limit for the general public is 100 mrem/yr.

B. MODELING PROGRAM OVERVIEW

Analysis and tracking of high energy electrons is a complicated task when the electron population becomes large. Use of complicated particle tracking software in conjunction with modeling software has allowed for complex shielding geometries to be analyzed. The program used in this project is FLUKA [22],[23], which is a Monte Carlo simulation program that allows for the understanding of high energy electron interactions and transport within various materials and geometries. Use of this program is for non-military applications and non-commercial applications; therefore, this research focuses on the shielding requirements of a design to be used for noncommercial, civilian applications.

C. FLUKA USAGE VALIDATION

The FLUKA program is a complicated program designed with many features that allow users to analyze the performance of shielding designs of specific geometries. Since this program is complex, the FLUKA physics engine is verified using a previous experiment conducted at the Naval Postgraduate School (NPS). The experiment consisted of energy deposition from a 100 MeV electron beam into a tank of water [24]. Measurements of the energy deposition at various distances within the water from the

beam were measured using a CaFl TLD. A FLUKA model was created to mimic the beam parameters and water geometry so that the predicted energy deposition values could be compared to the experimental ones.

Figure 19 displays the results from FLUKA of the radial dose generated in the model of a 100 MeV electron beam penetrating the water tank. The graph (Figure 19) also provides a visualization of the attenuation characteristics of electrons in water. This figure was then compared to experimental data points that were translated from the NPS report. The report states that the data points from the experiment have up to 20% error in there recorded values. These recorded dose values from the report were taken from various off-axis distances. The model results were averaged at the specific distances matching the experimental distances from the report. The excellent agreement shown in Figure 20 both on and off-axis at various distances in the water tank indicate that the performance of the FLUKA engine and the methodology of modeling were correct. These results now show that we can confidently continue with the shielding design studies.

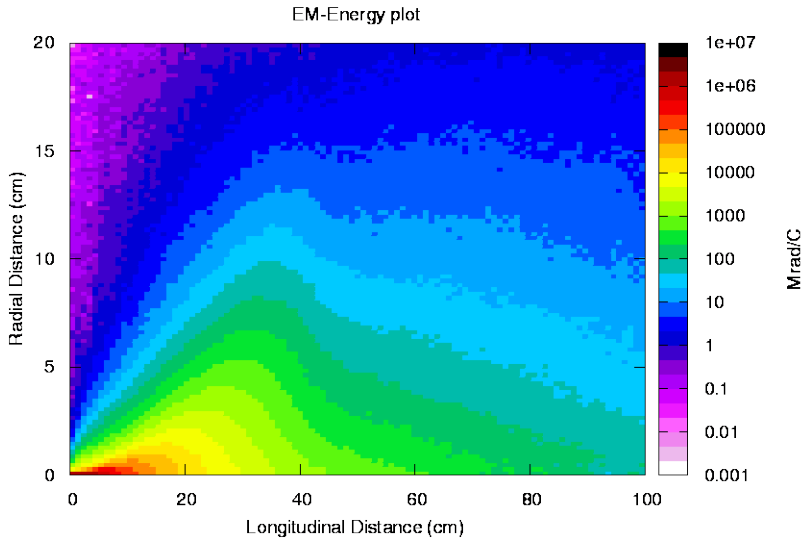

Figure 19. Dose values 100 MeV electron beam in water with FLUKA.

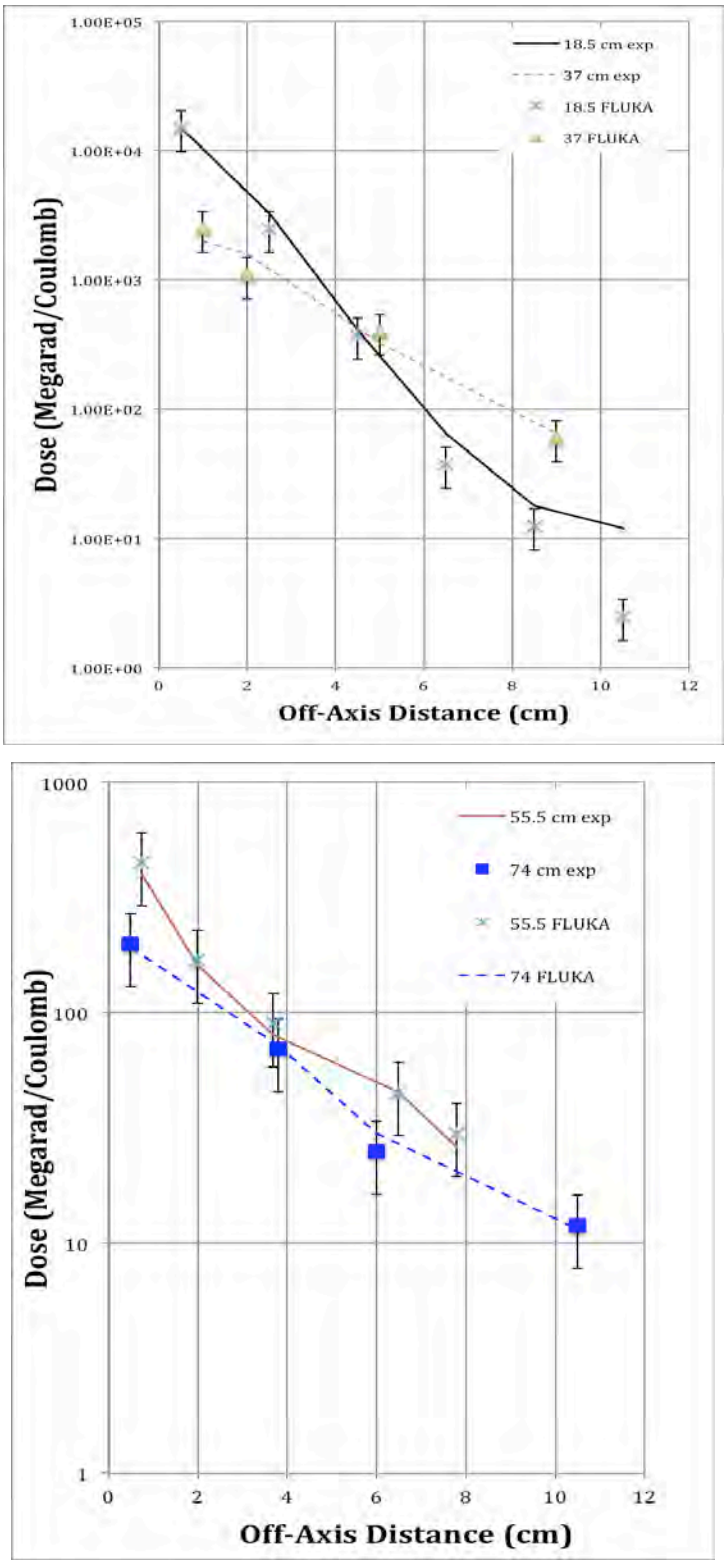

Figure 20. Graphs show comparison between the experiment and FLUKA at various distances within the water tank [After 24]

THIS PAGE INTENTIONALLY LEFT BLANK

VII. SHIELD MODELING FOR ENERGY RECOVERY LINAC (ERL) FEL

A. GENERAL MODEL DESIGN PARAMETERS

The goal of the different shielding designs is to understand the relationship between the halo electrons lost and the shielding required to protect personnel in the near proximity. The shielding required will also be determined by the amount of radiation that would be allowed on the outside of a vault. Using the radiation limits established by the NRC and DOE for facility workers of 5 rem/yr with a 2000 hr/yr exposure time equates to an allowable exposure rate of 2.5 mrem/hr. In order to allow for modeling and calculational errors of the radiation exposure rate, the limit was set to 2 mrem/hr (80% of allowable). It is noted that other research facilities have established radiation limits outside the shield based on the lower general public limit of 100 mrem/yr. We chose the higher value to give the most flexibility in our shield designs and with the intention that some of these designs may be mobile or in isolated areas. Restricting access outside the shield to non-facility workers during operation will allow for higher exposure limits outside the shielding.

The basic model of the FEL uses a single beam pipe contained within a vault enclosure. This configuration was chosen as the "worst case scenario" in determining the acceptable amounts of halo loss. It is understood that an Energy Recovery Linac (ERL) FEL does contain other components that can intercept halo electrons. Most of the other beamline components of concern (the undulator, for example) have larger material thicknesses as compared with the beam pipe. If the material has substantial thickness it will start to have some self-shielding properties of the radiation being produced within the material. This self-shielding effect causes thicker materials to absorb more of the radiation being produced compared to thinner materials. The beam pipe used in the models has a diameter of 4.5 cm and wall thickness of 0.25 cm and will have little self-shielding effect.

Halo electrons that collide with the beam pipe can scrape secondary electrons off the interior wall and introduce them into the electron population contained within the

beam pipe. These secondary electrons will not be at same energy level as the general electron population traveling in the beam pipe. This difference can have an effect when the lower energy electrons enter into the bending magnets. The lower energy electrons might collide with the inner surface of the beam line and not make it around the bend. An end cap was inserted in our model on the end of the beam pipe to simulate this event. The wall thickness of the end cap was set to the same wall thickness as the straight section of the beam pipe (0.25 cm). The length of the beam pipe is 4 m and allows for the halo electrons to spread over approximately 1 m of the beam pipe due to divergence. Another consideration in the length of the beam pipe was to have it long enough so that the secondary electrons could be produced and have some impact on the results.

The electron beam of the FEL will have a initial position of 50 cm from the beginning of the beam pipe and directed along the pipe. Table 2 lists the other parameters used for the electron beam halo. The beam energy is 100 MeV with a cylindrical shape of 3 mm radius and 30 mrad angular spread. These values were chosen to create a condition for the halo electrons to interact with the beam pipe to evaluate the shielding requirements.

Beam Radius	0.3 cm
Beam Shape	Cylinderical
Beam Energy	100 Mev
Beam Divergence	30 mrad

Table 2. Electron beam halo parameters

B. COMPARTMENT BULKHEAD ANALYSIS

1. Concrete Only

As mentioned previously, a common material used at accelerator facilities for shielding is concrete. In this model, the thickness of the concrete was varied and resulted in changes in the amount of radiation dose received outside the shielding. These radiation dose rates were then correlated to the amount of acceptable halo electron loss

that would keep the outside total radiation exposure to < 2 mrem/hr. In designing the FEL vault, a cyclindrically symmetric shape was used as this simplified the design and visualization of the results; centered within the vault was the beam pipe described above. The wall thickness in this model was varied from 100 cm to 200cm in 20 cm increments as shown in Figure 21.

Figure 21. Concrete-only model in FLUKA with 20 cm partitions for additional shielding (Light blue – Air; Purple – Concrete; Dark blue –Water)

In Figure 22 shows the resultant radiation distribution. The strong forward focusing of the photon radiation, and a more isotropic distribution of neutron radiation is observed. The radiation level was measured on the outside of the downstream wall with a 30 cm thick detector of water (representing a person) and placed 1 cm outside from the outer surface of the shielding.

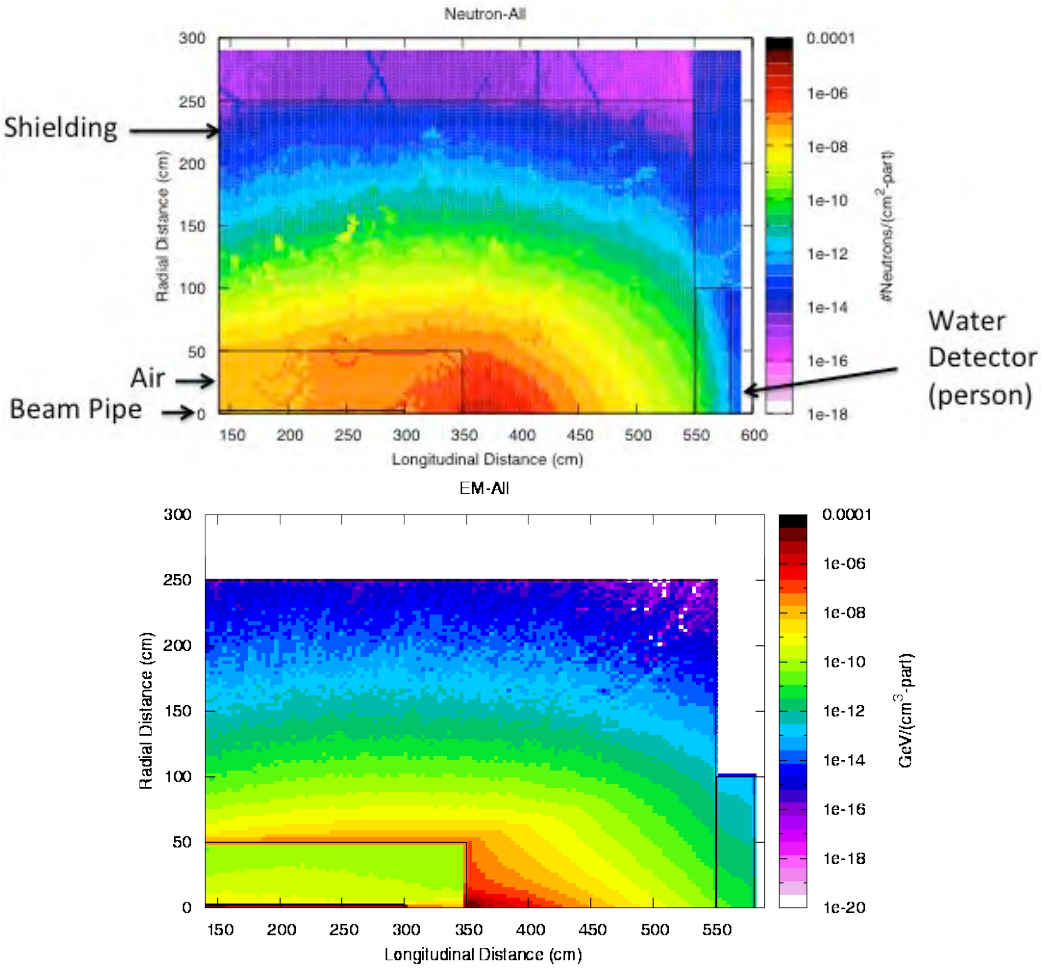

Figure 22. (Top) Number of neutrons per cm^2-primary. (Bottom) Energy deposition from photons. Both graphs use 200 cm of concrete shielding.

Figure 23 shows the dose reported in Sieverts per primary particle (pSv/part) received in the detector (person) after 200 cm of concrete. A sievert is the international standard for dose equivalent (1 Sv = 100 rem).

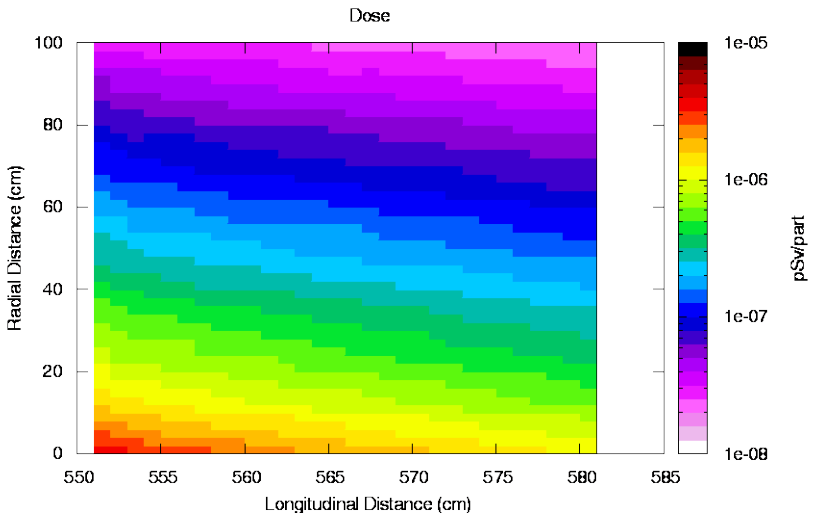

Figure 23. FLUKA dose measurement in water (person) after 200 cm concrete.

The highest dose value obtained from the graph was used as the whole body dose due to penetration being at least 2 cm within the water detector. Figure 24 shows the results of the measurements taken from the increase in shielding from 1 m to 2 m. The maximum amount of halo current allowed (based on not exceeding 2 mrem/hr) is plotted in Figure 24 as the concrete shielding thickness is varied from 100 cm to 200 cm. The lost halo current allowed is only ~1.5 pA if only 1 m of concrete shielding is used. The lost halo current allowed increases to 250 pA if 2 m of concrete is used.

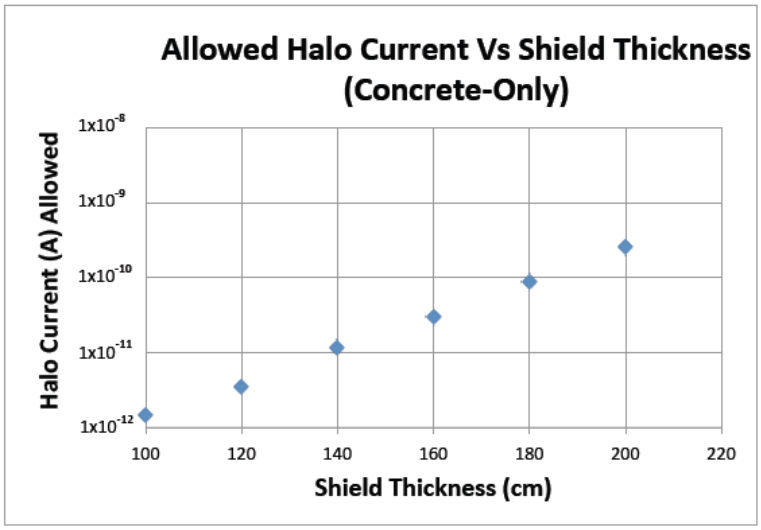

Figure 24. Halo current loss versus shield thickness for 100–200 cm of concrete

These results were compared to hand calculations using ~100 cm of concrete shielding. The current of the halo electrons being lost was assumed to be 1 μA and with a radius of 2.25 cm. A thumb rule was used to convert the high energy electrons that collide with a thick material to a dose rate (dD/dt). This thumb rule is for electrons with E_0> 20 MeV. The results of the calculations were as follows [17]:

$$\frac{dD}{dt} \approx 300 E_0 \text{ [(Gy hr}^{-1}\text{)(kW m}^{-2}\text{)}^{-1}\text{]}, \tag{42}$$

$$\frac{dD}{dt} = 300(100) = 3\times 10^4 \text{ [(Gy hr}^{-1}\text{)(kW m}^{-2}\text{)}^{-1}\text{]} \approx 4.7\times 10^7 \text{mrem/hr},$$

where E_0 is the initial electron energy in MeV and Grey (Gy) is the international standard for dose absorbed (1 Gy = 100 rad). The half value thickness of concrete is 15 cm for 100 MeV electrons obtained using Figure 18. Using the half value thickness a dose rate can be calculated for outside the shielding using (41) as follows:

$$H_{shielded} = \left(0.5^{x/x_{1/2}}\right) H_{unshielded},$$

$$H_{shielded} = (0.5^{100/15}) 4.7\times 10^7 \, mrem/hr \approx 4.7\times 10^5 \, mrem/hr,$$

where H is the photon dose rate (shielded and unshielded), x is the thickness of the material, and $x_{1/2}$ is the half-valued thickness. The calculations were then compared with values obtained from the model in Table 3.

Calculated Results (100 cm Concrete)	Model Results (100 cm Concrete)
$4.7\text{x}10^5$ mrem/hr	$1.34\text{x}10^6$ mrem/hr

Table 3. Comparison of calculated and FLUKA model results

Differences between the two results can be associated with the fact that the detectors in this model integrate the total of all the types radiation received and reports a cumulative result. The hand calculated results only use a photon dose since it is the dominant radiation source. Even with these differences, the simulated and hand calculated estimates are the same order of magnitude; this provides verification that the model results are reasonable.

2. Lead-Concrete Shielding

The next shielding configuration analyzed the effectiveness of using lead in combination with concrete shielding. Using lead prior to the concrete allows for attenuation of the high energy photons and electrons. The concrete is used after the lead to attenuate and absorb the photoneutrons produced in the lead. This model evaluated the thickness of the lead/concrete shielding and compared it with the 200 cm of concrete. The 100 cm of concrete used in this model remained fixed. The lead shielding was added to the interior of the vault wall downstream of the beam pipe. Thickness of the lead shielding was varied from 0 to 15 cm in 3 cm increments. Placement of the detector remained in the same position as in the concrete-only model (Figure 25).

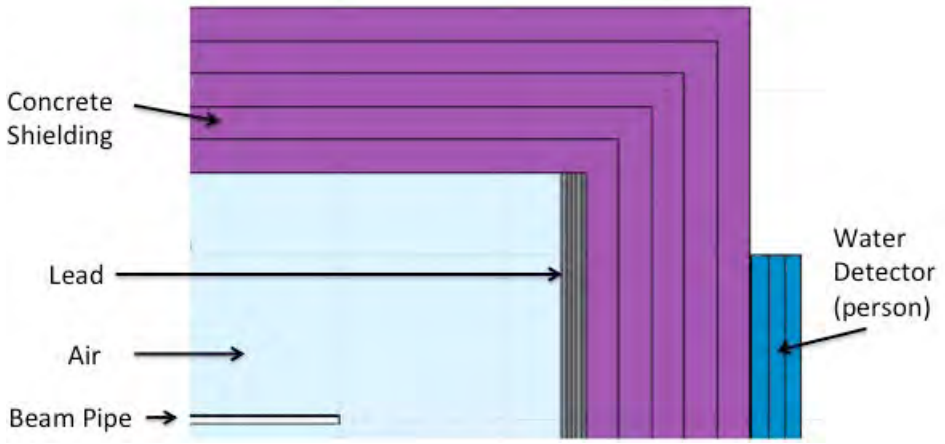

Figure 25. 100 cm Concrete shielding model with lead shielding. (Light blue – Air; Grey – Lead; Purple – Concrete; Dark blue –Water)

Figure 26 shows that the photon radiation has a strong forward focusing while the neutrons in the graph (top) show the lead having a stronger scattering effect than seen in Figure 22. Thickness of the lead shielding in Figure 26 is 9 cm. The photon graph in Figure 26 (bottom) can be compared to Figure 22 after ~100 cm of concrete and shows the photon distributions starts to look similar. This similarity can be confirmed by comparing the lead and concrete "tenth thicknesses," which is the amount of material that is required to reduce the dose rate by 1/10 of the original value. The tenth thickness for concrete is ~50 cm (Figure 18) and with the 100 cm of concrete would result in

approximately two tenth thicknesses. Lead has a tenth thickness of ~ 4.5 cm, so two tenth thicknesses of lead is approximately equal to 100 cm of concrete.

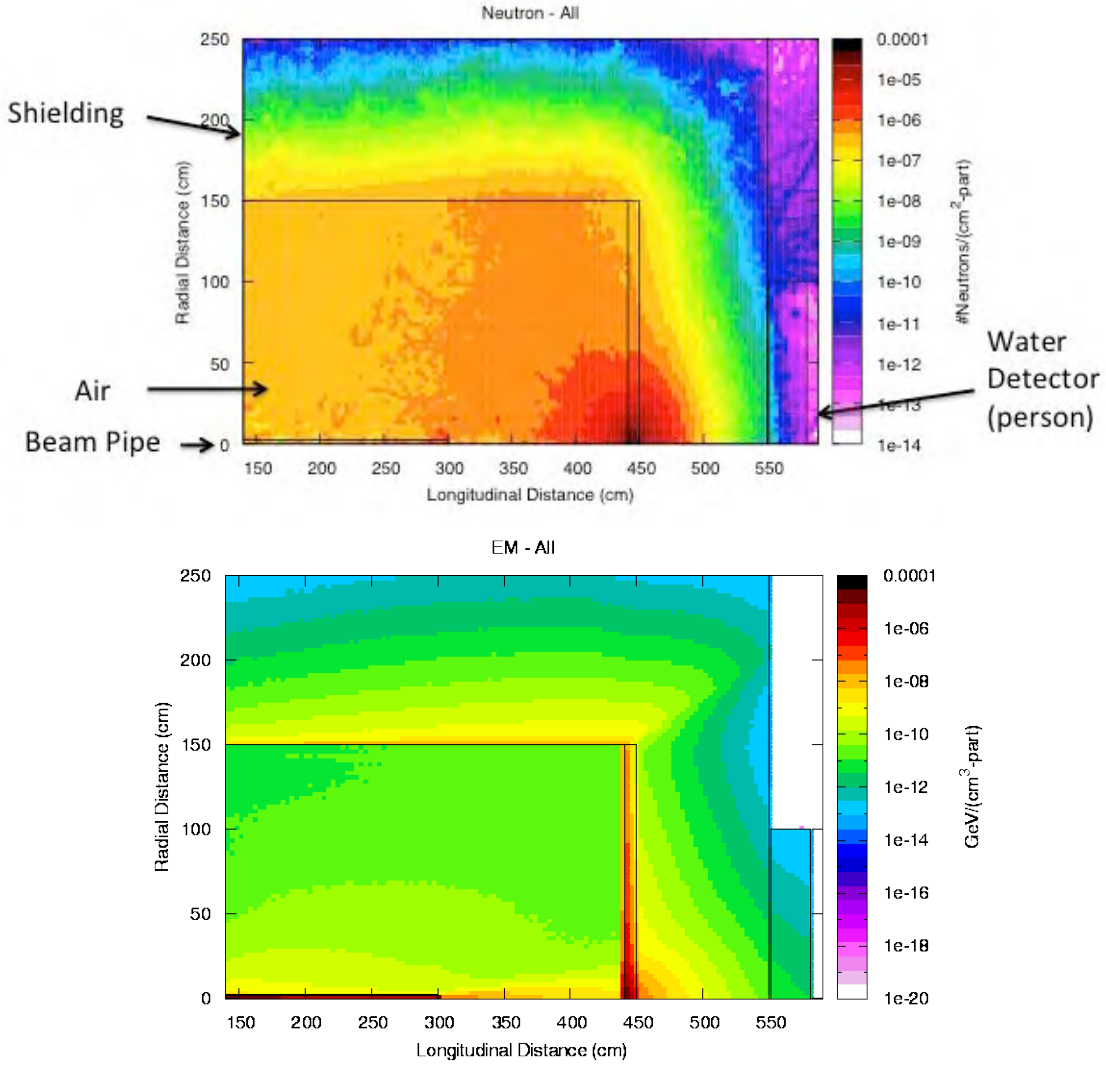

Figure 26. (Top) Number of neutrons per cm^2-primary. (Bottom) Energy deposition from photons. Both graphs using 9 cm of lead followed by 100 cm of concrete.

The radiation levels were measured with the same detector configuration as used in the concrete-only model. Figure 27 shows the dose (pSv/part) received in the detector with 9 cm of lead and 100 cm of concrete.

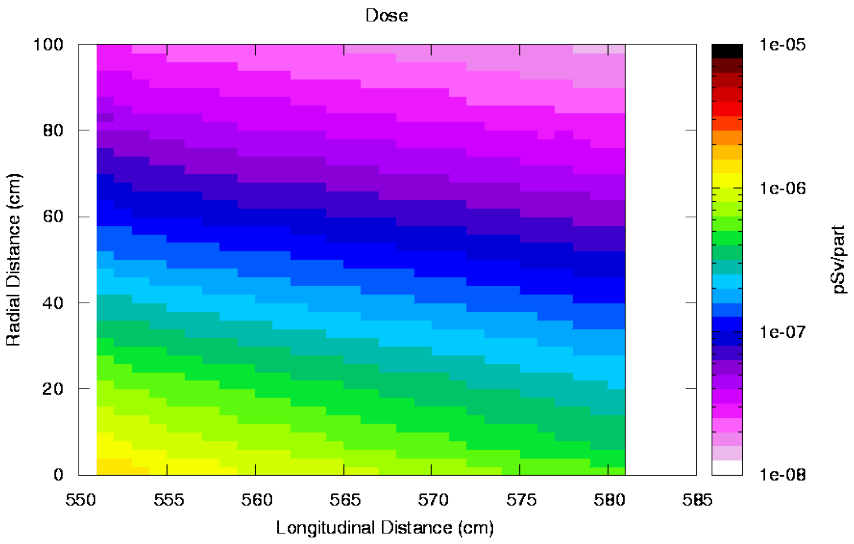

Figure 27. Total dose (pSv/part) outside downstream wall for 9 cm lead and 100 cm concrete

The maximum amount of halo current allowed in this case (based on not exceeding 2 mrem/hr) is plotted in Figure 28 as the lead shielding thickness is varied from no lead to 15 cm with an additional 100 cm of concrete. The lost halo current allowed is only ~1.5 pA if only 1 m of concrete shielding is used. The lost halo current allowed increases by almost 6000 times to 8.9 nA if 15 cm of lead is used in addition to the concrete.

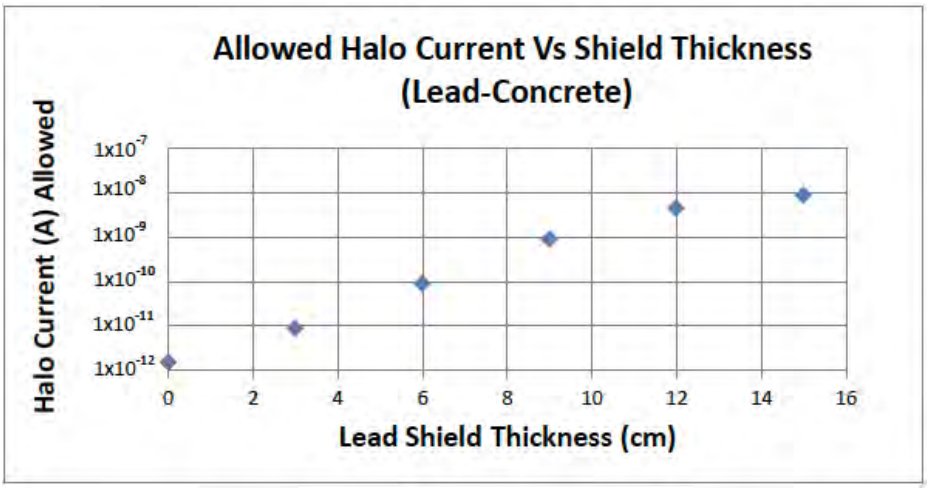

Figure 28. Maximum halo current loss versus varying thicknesses of lead followed by 100 cm of concrete

C. LOCALIZED SHIELDING

The primary shielding in most ERL FEL facilities is the vault walls. Use of an ERL FEL in the future may require that the FEL be mobile, so it may not be desirable to have thick heavy walls. This section will assume that the ERL FEL can be compartmentalized to fit into a series of semi-trailers. The walls of the trailer are assumed to be 0.635 cm thick carbon steel. These walls are thicker than the traditional trailer walls and were chosen based on the need for structural support for the trailer containing the FEL. Some of the constraints associated with using a trailer to house the FEL are the width and weight of the trailer.

One of the ways to address the weight and size restrictions is to have localized shielding in only these areas that halo electron loss would most likely occur. Using localized shielding could eliminate or dramatically reduce the overall shielding required on the walls of the trailer. The models will utilize two primary materials for the localized shielding. One of them is the standard lead shielding used previously and the other material is a 30% borated polyethylene (SWX-210) from Shieldwerx [25]. This material required creating it within FLUKA based on the manufacture's material specifications. The localized shielding shapes are modeled as cylinders surrounding the beam pipe for simplification of the modeling.

Weight savings from utilizing localized shielding versus exterior shielding can be evaluated using the different densities of the materials. The density is 2.3 g/cm^3 for concrete, 1.12 g/cm^3 for borated-poly, and 11.34 g/cm^3 for lead. For the same given volume of shielding materials, a 50%/50% arrangement of borated-poly/lead by volume would have approximately three times more weight than concrete. Use of localized shielding allows for the significant reduction of the volume of material required. Even with using the more dense materials, it would weigh less overall compared to using lighter materials on all the trailer walls. More weight savings can be gained from having the localized shielding in areas more prone to higher radiation levels from lost halo electrons. A consequence of using localized shielding is that the components requiring shielding may be more difficult to access for repair or maintenance.

1. Borated-Poly and Lead, Alternating

The first localized shielding configuration was to place a 7.5-cm thick section of borated-poly next to the beam pipe. A 7.5-cm thick piece of lead was placed outside of the borated-poly and the materials were alternated giving a final shielding thickness of 75 cm (Figure 26). This configuration was chosen with the understanding that the borated-poly has poor shielding characteristics for high energy electrons and photons, but better for neutrons. The purpose of this model was to see the effects of placing high Z materials after the lower Z materials. An additional water detector (person) was placed on the side of this model to see if the localized shielding had any effect on the radiation patterns.

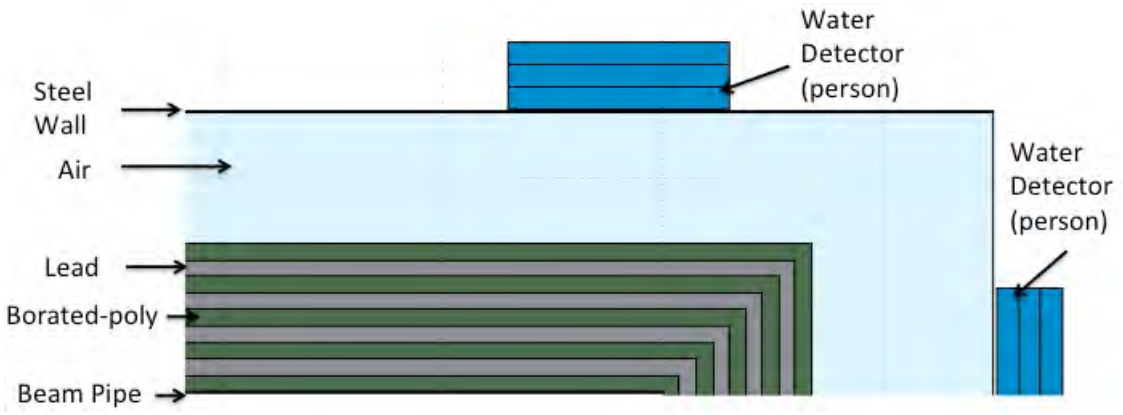

Figure 29. Model layout of localized shielding with alternating borated-polyethylene and lead. (Green – borated-poly; Gray – Lead; Light Blue – air; Dark Blue – Water)

Figure 30 shows that the photons and neutrons still maintain a strong forward focusing of the radiation. The alternation of the lead and borated-poly has significant impact on the both the neutrons and photons. This impact can be accounted for due to the attenuation of the electrons/photons from the high Z material (lead) and of the photoneutrons from the low-Z material (borated poly). Furthermore, the layers of lead surrounding the borated-poly also help to attenuate capture gamma photons.

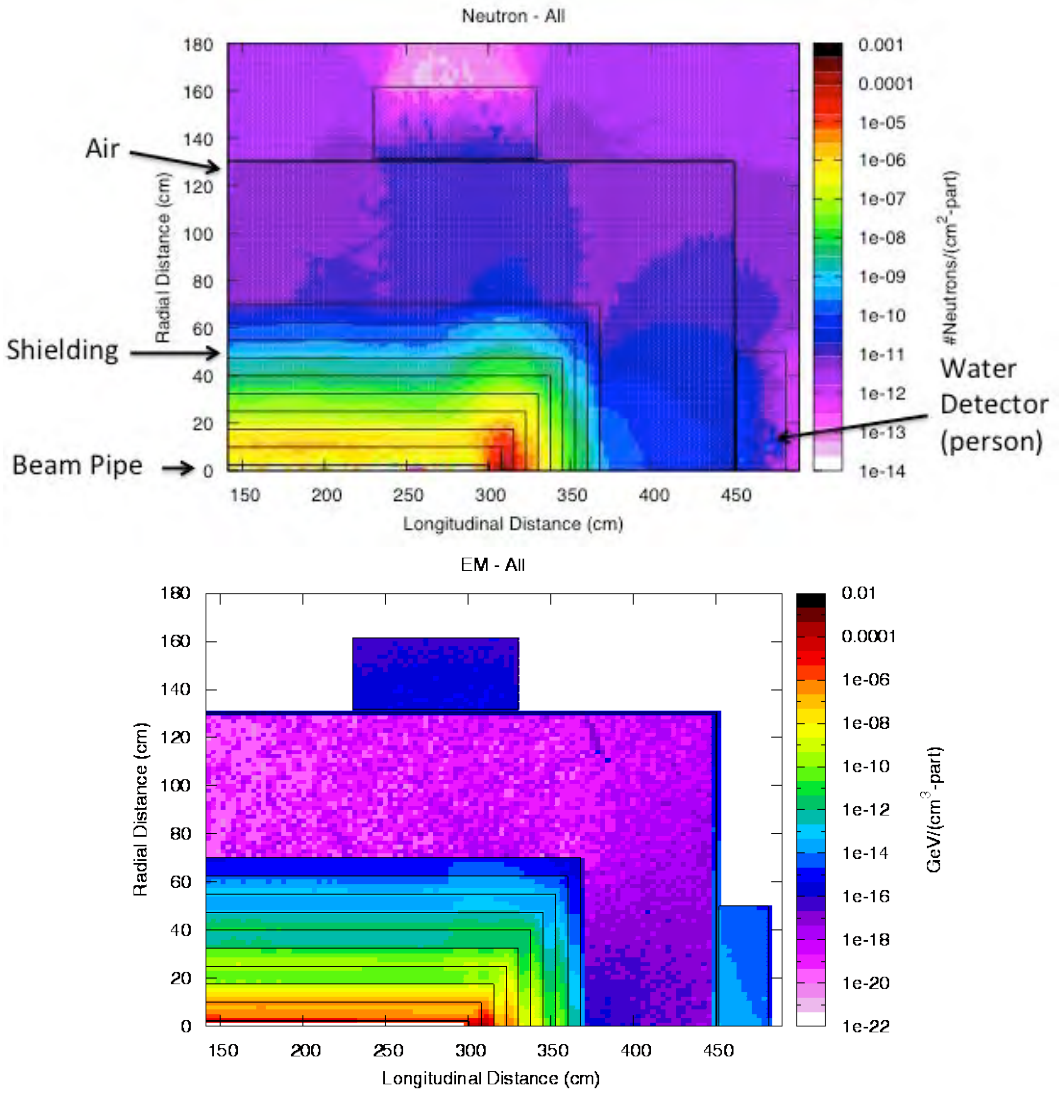

Figure 30. (Top) Number of neutrons per cm^2-primary. (Bottom) Energy deposition from photons. Both graphs use 7.5 cm of borated-poly followed by 7.5 cm of lead that alternates to a total of 75 cm.

Radiation measurements were performed after each 15 cm section of borated-poly/lead shielding was inserted. The values were then collected and compared with the other values obtained over the entire 75 cm of shielding (Figure 31). Radiation values from the side detector confirmed that the downstream wall was still the primary concern.

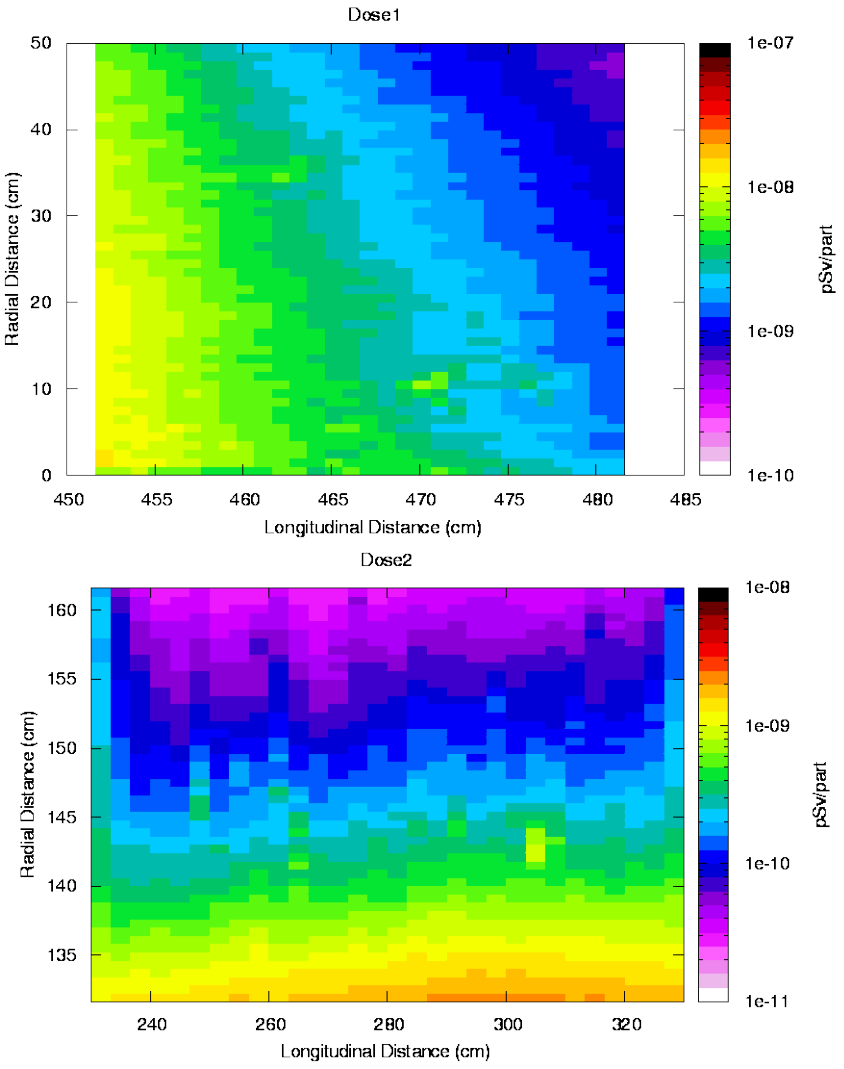

Figure 31. (Top) Total dose (pSv/part) outside downstream wall. (Bottom) Total dose (pSv/part) outside side walls. Both graphs use 7.5 cm of borated-poly followed by 7.5 cm of lead that alternates to a total of 75 cm.

The maximum amount of halo current allowed in this case (based on not exceeding 2 mrem/hr) is plotted in Figure 32 as the borated-poly/lead thickness (50%/50%) is varied from 15 cm to 75 cm. The lost halo current allowed is only ~1.1 pA if only 15 cm of borated-poly/lead shielding is used. The lost halo current allowed increases to 0.25 μA if 75 cm of borated-poly/lead is used. Comparing the maximum halo loss current of 0.25 μA (localize) to 0.25 nA (concrete-only) shows that the heavier and

more effective shielding materials should be used. As mentioned, the overall weight will be less utilizing localized shielding compared to general wall shielding.

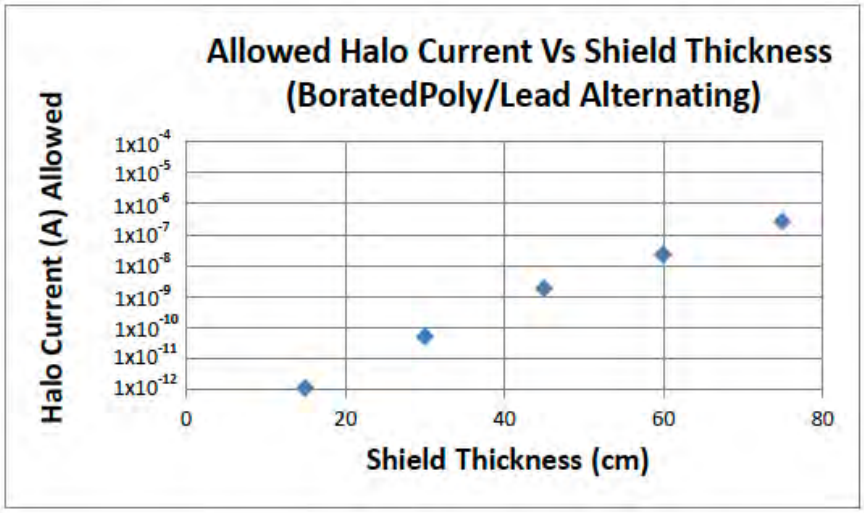

Figure 32. Maximum halo current loss versus shield thickness for 7.5 cm of borated-poly followed by 7.5 cm of lead that alternates to a total of 75 cm.

2. Lead and Borated-Poly, Alternating

The next localized shielding configuration was to switch the order of the lead and borated-poly shielding materials from the previous model. Thickness of the shielding materials was maintained at 7.5 cm for each section and the overall localized shielding thickness stayed at 75 cm as shown in Figure 33.

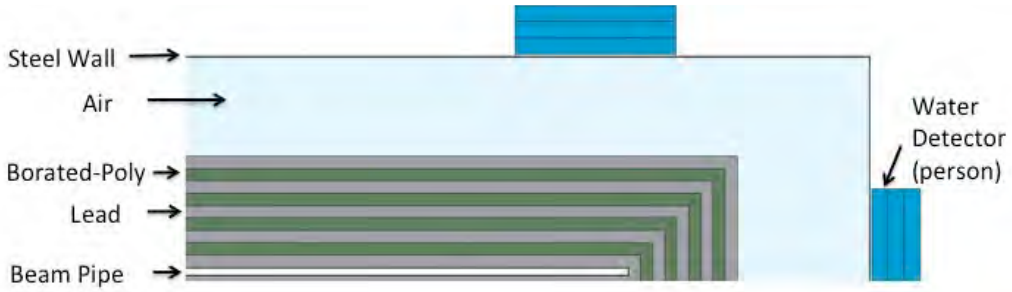

Figure 33. Model layout of localized shielding with alternating lead and borated-polyethylene (Green – borated-poly; Gray – Lead; Light Blue – air; Dark Blue – Water)

Figure 34 shows that the photons and neutrons still have a strong forward focusing of the radiation. The alternating of the lead and borated-poly still maintains a strong impact on both the neutrons and photons. There appears to be some differences between Figure 30 and Figure 34. These differences are believed to be due to more photons being attenuated since the lead is now next to the beam pipe. Attenuating the photons early allows for the borated-poly to be more effective at attenuating the photoneutrons. This is due to photoneutrons being produced prior the first layer of borated-poly. Therefore, more borated-poly is exposed to the photoneutron flux and is more effective than the previous model.

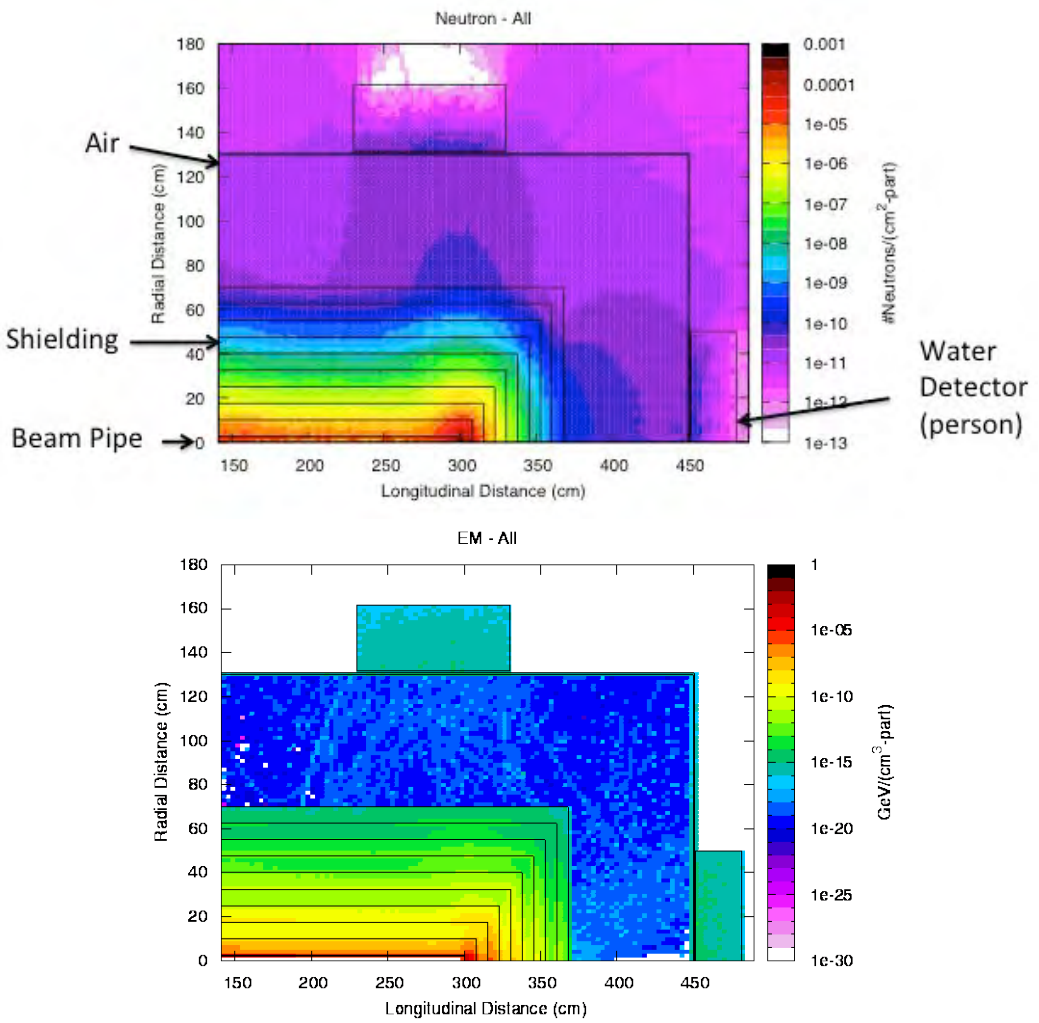

Figure 34. (Top) Number of neutrons per cm^2-primary. (Bottom) Energy deposition from photons. Both graphs use 7.5 cm of lead followed by 7.5 cm of borated-poly that alternates to a total of 75 cm.

Radiation measurements were performed after each 15 cm section of lead/borated-poly shielding was inserted (Figure 35). The values were then collected and compared with the other values obtained over the entire 75 cm of shielding.

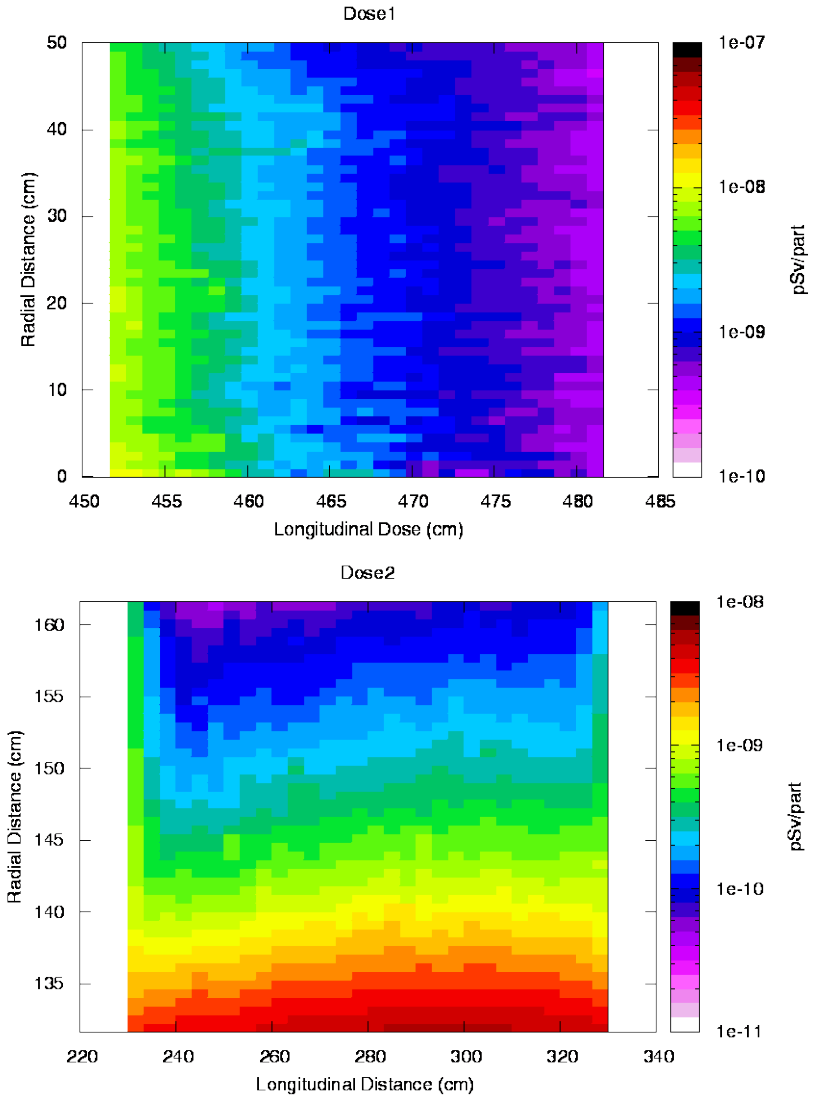

Figure 35. (Top) Total dose (pSv/part) outside downstream wall. (Bottom) Total dose (pSv/part) outside side walls. Both graphs use 7.5 cm of lead followed by 7.5 cm of borated-poly that alternates to a total of 75 cm.

The maximum amount of halo current allowed in this case (based on not exceeding 2 mrem/hr) is plotted in Figure 36 as the lead/borated-poly thickness (50%/50% by volume) is varied from 15 cm to 75 cm. The lost halo current allowed is

only ~1.1 pA if only 15 cm of lead/borated-poly shielding is used. The lost halo current allowed increases to 0.71 μA if 75 cm of lead/borated-poly is used. Comparing Figure 32 and 36 shows a 64% difference in the effectiveness of the shielding based on which material was placed first against the beam pipe. This shows the importance of the higher Z material and the effectiveness of attenuating the higher energy electrons/photons.

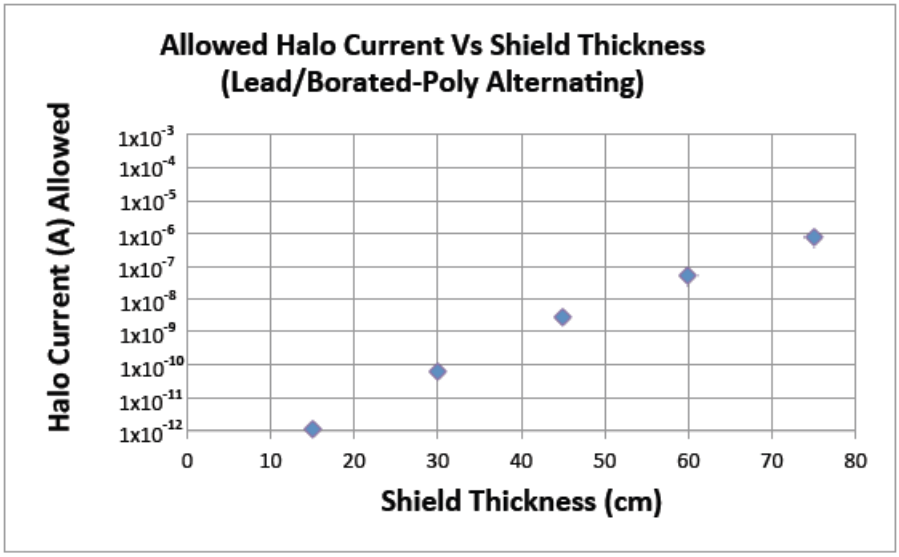

Figure 36. Maximum halo current loss versus shield thickness for lead/borated-poly alternating

3. Lead and Borated-Poly, Nonalternating

The benefit of the lead shielding being the first material is now established. This model uses the same total thickness of shielding materials as the previous localized shielding models but without the alternating pattern. The purpose of this model is to compare its effectiveness to the previous localized shielding models. A 37.5-cm thick section of lead shielding was placed immediately next to the beam pipe and followed by another 37.5-cm thick section of borated-poly (Figure 37). The total amount of shielding thickness is the same as the previous cases.

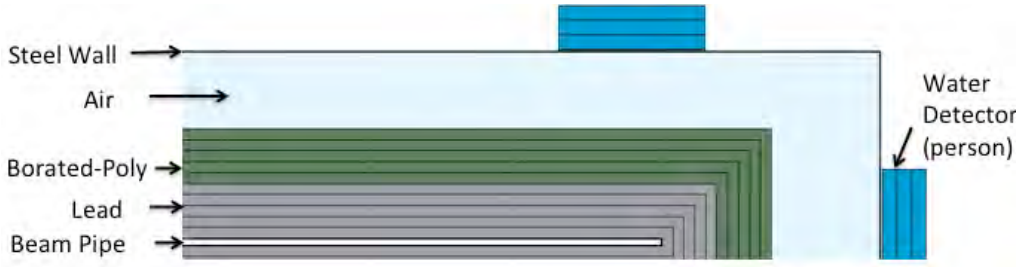

Figure 37. Model layout of localized shielding with 37.5 cm of lead followed by 37.5 cm of borated-polyethylene (Green – borated-poly; Gray – Lead; Light Blue – air; Dark Blue – Water)

Figure 38 shows the radiation patterns for the photons and neutrons. The neutron graph (top) shows a strong neutron fluence being produced due to the large amount of high Z material close to the beam pipe in this model.

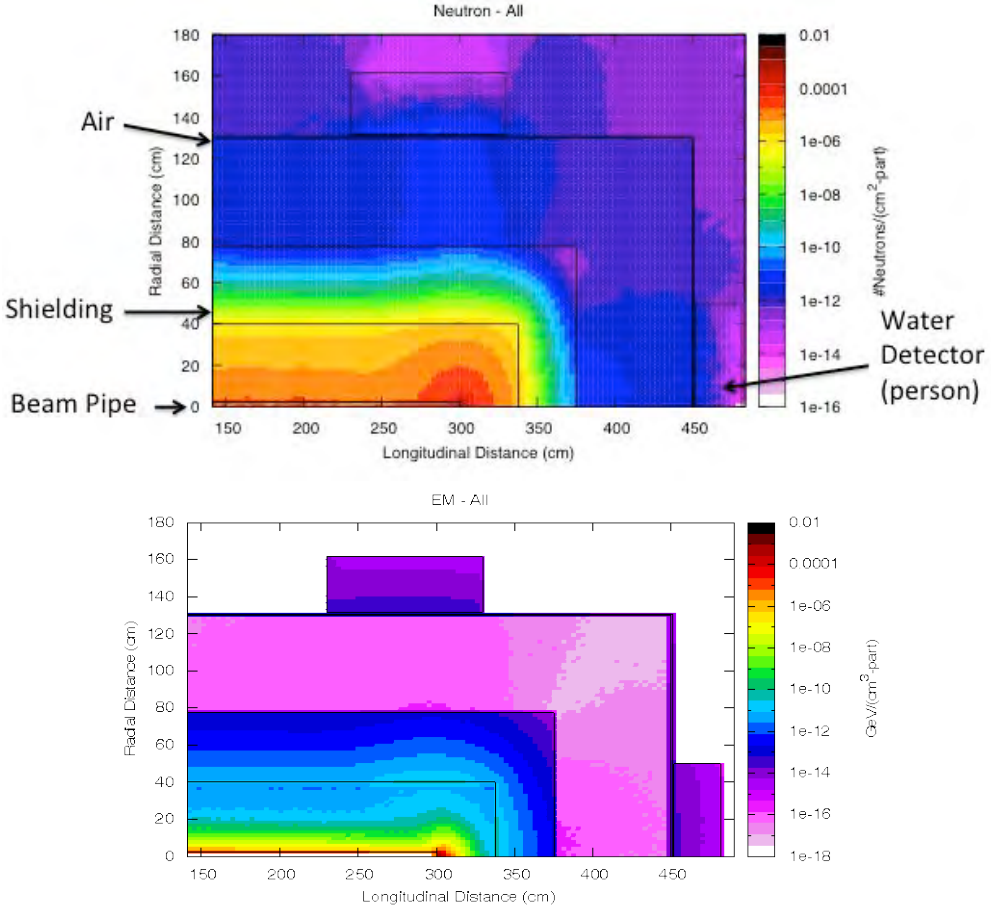

Figure 38. (Top) Number of neutrons per cm^2-primary. (Bottom) Energy deposition from photons. Both graphs use 37.5 cm of lead followed by 37.5 cm of borated-poly.

Dose values obtained in this configuration resulted in the side detector and downstream detector being approximately equal as shown in Figure 32. It is believed that the stronger dose to the side detector can be attributed to the increase in the amount of capture gammas and a more isotropic distribution of the photoneutrons produced.

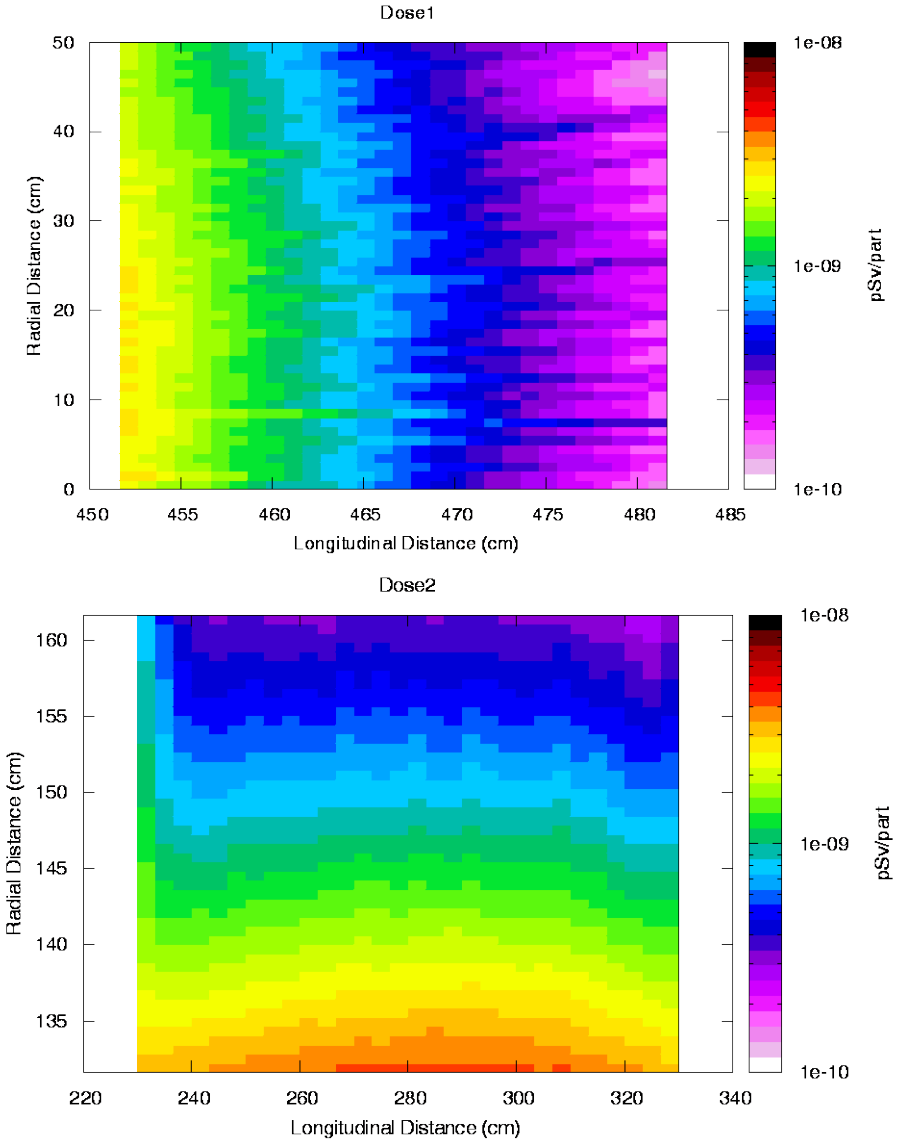

Figure 39. (Top) Total dose (pSv/part) outside downstream wall. (Bottom) Total dose (pSv/part) outside sidewall. Both graphs using 37.5 cm of lead followed by 37.5 cm of borated-poly configuration.

The effectiveness of this shielding configuration was evaluated by reducing the shielding material for both the lead and borated-poly keeping the percentage of each material remained the same during each simulation run. The maximum amount of halo current allowed in this case (based on not exceeding 2 mrem/hr) is plotted in Figure 40 as the lead/borated-poly thickness is varied from 15 cm to 75 cm of the stated shielding configuration. The lost halo current allowed is only ~1.1 pA if only 15 cm of the lead/borated-poly shielding is used. The lost halo current allowed increases to 0.3 μA if 75 cm of lead/borated-poly is used.

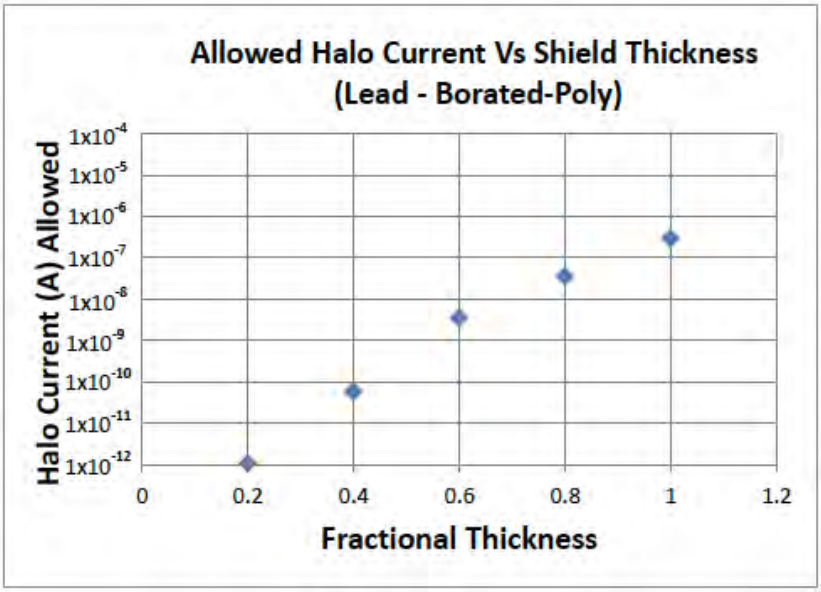

Figure 40. Maximum halo current loss versus shield thickness for 37.5 cm of lead followed by 37.5 cm of borated-poly configuration

4. Lead – Borated-Poly – Lead, Nonalternating

The previous model showed that with the thicker high Z material next to the high energy photon source, more photoneutrons were produced. A higher production of photoneutron will result in a higher dose rate from capture gammas, if there is no additional high-Z shielding. This model will continue to use the same total thickness of shielding materials as the previous localized shielding models. The purpose of this model is to modify the previous model in C.3 by moving 15 cm of the lead shielding to the outside of the borated-poly (Figure 41). This will allow for attenuation of the lower energy capture gammas produced from the photoneutron production.

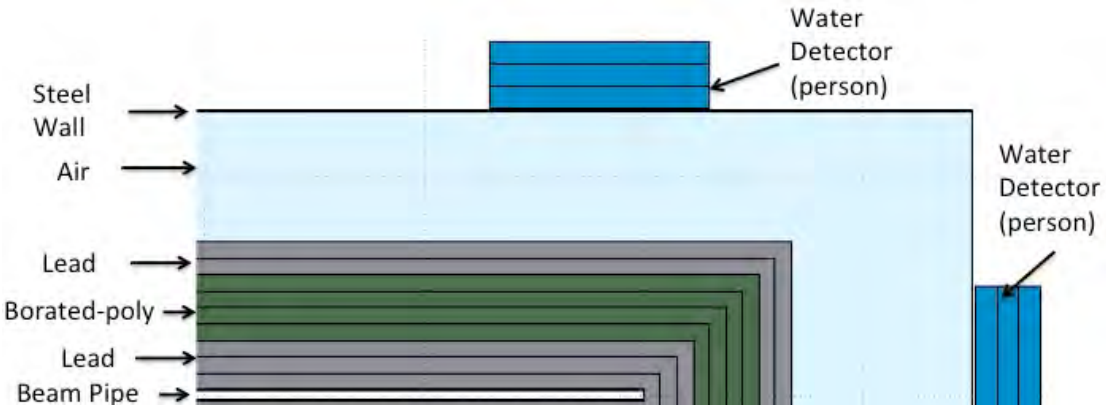

Figure 41. Model layout of localized shielding with 22.5cm lead/37.5 cm borated-poly/15 cm lead configuration (Green – borated-poly; Gray – Lead; Light Blue – air; Dark Blue – Water)

Figure 42 shows the radiation pattern for the photons and neutrons produced from the high energy electrons colliding with the various materials. The neutron graph (Figure 38-top) shows that the strong fluence produced is approximately the same value as shown in Figure 42 (top). Comparing Figure 38 and Figure 42, photon energy deposition shows that there is a difference due to the lead shielding being placed on the outside of the borated-poly.

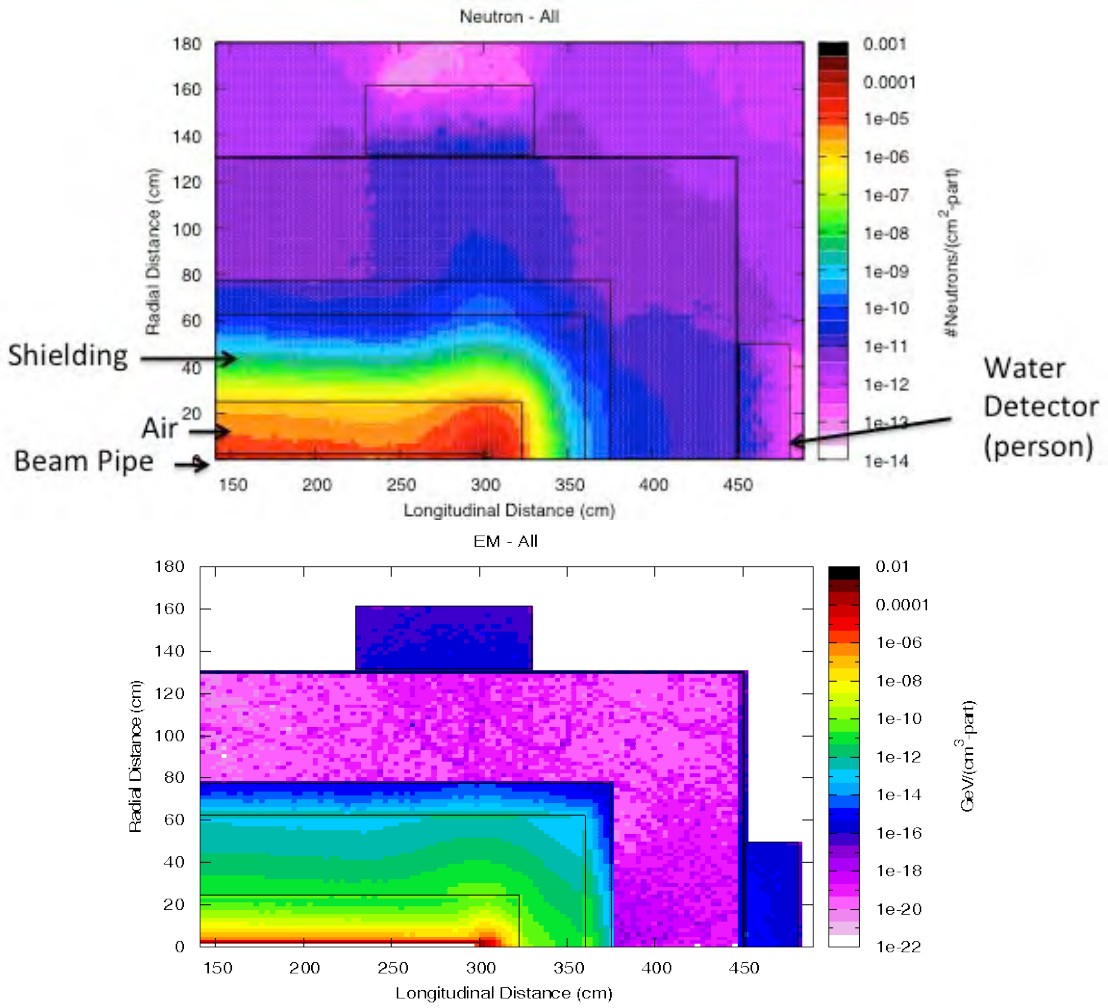

Figure 42. (Top) Number of neutrons per cm^2-primary. (Bottom) Energy deposition from photons. Both graphs use 22.5 cm of lead followed by 37.5 cm of borated-poly followed by15 cm of lead.

Dose values obtained in this configuration are shown in Figure 43. The dose values between the side detector and the downstream detector show the effect of moving the lead material to the outside of the borated-poly. The small difference between the two detectors can be attributed from the capture gammas having lower energy as compared with the bremsstrahlung photons and contributes less to the total dose.

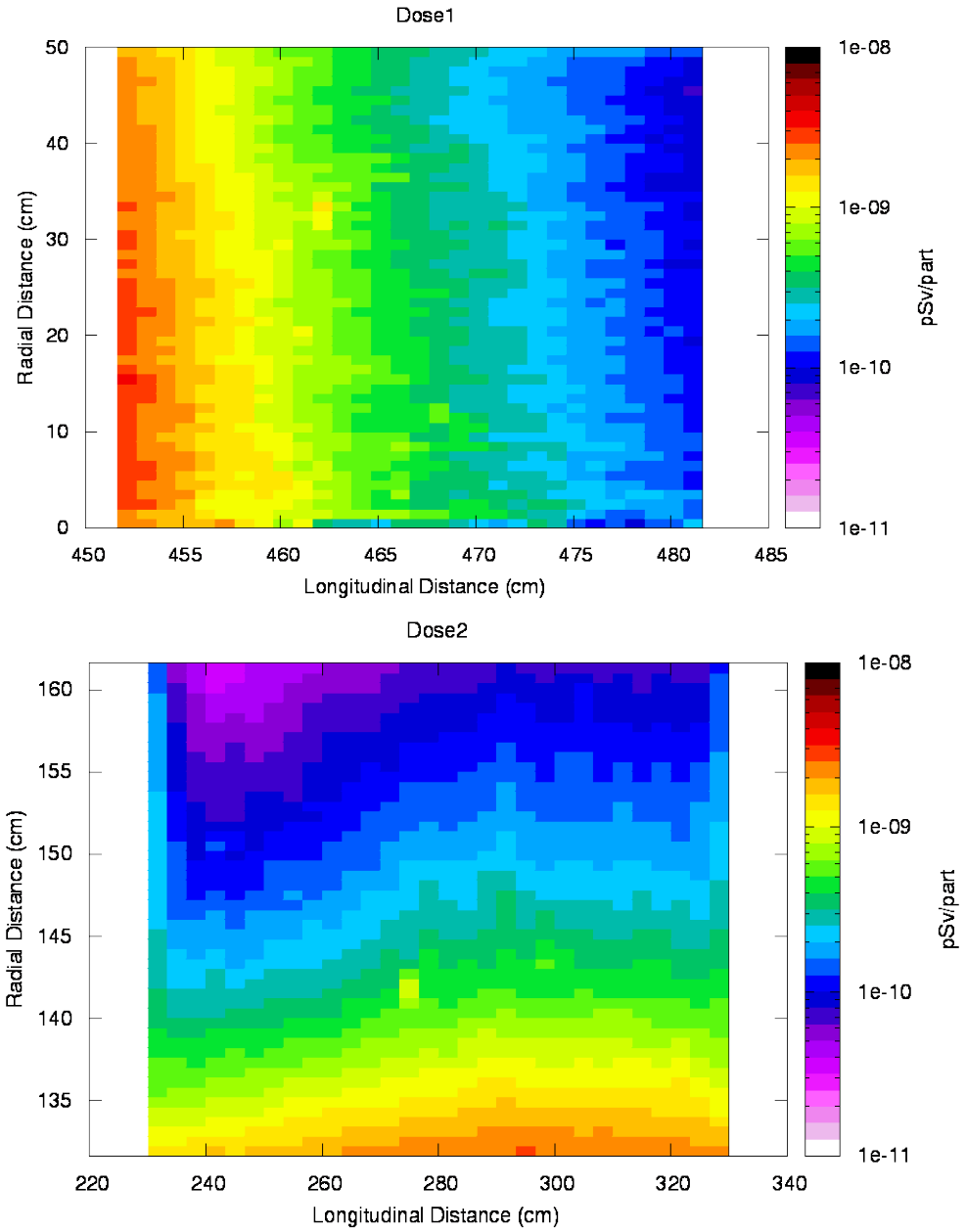

Figure 43. (Top) Total dose (pSv/part) outside downstream wall. (Bottom) Total dose (pSv/part) outside sidewalls. Both graphs using 22.5 cm of lead followed by 37.5 cm of borated-poly followed by 15 cm of lead.

The effectiveness of this shielding configuration was evaluated by reducing the percentage of shielding material for both the lead and borated-poly. The configuration of the shielding remained the same during each simulation run. The maximum amount of

halo current allowed in this case (based on not exceeding 2 mrem/hr) is plotted in Figure 44 as the lead/borated-poly/lead thickness is varied from 25 cm to 75 cm of the stated shielding configuration. The lost halo current allowed is only ~16.2 pA if 25 cm the lead/borated-poly/lead shielding is used. The lost halo current allowed increases to 0.3 μA if 75 cm of borated-poly/lead is used.

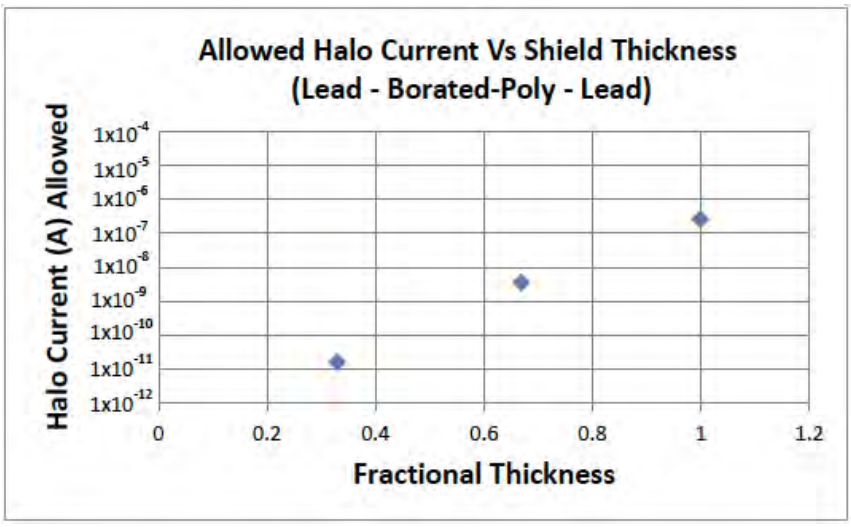

Figure 44. Halo current loss versus shield thickness for 22.5cm lead/37.5 cm borated-poly/15 cm lead configuration. Other data represent percentage of the original 75 cm thickness.

These various model configurations show that some are more effective shields than others. Table 4 shows the maximum halo current allowed for 75 cm of shielding for the localized shielding models.

Maximum halo current allowed for 75 cm of shielding	
Model	Maximum Halo Current Allowed
Borated-poly/Lead (alternating)	$2.5x10^{-7}$
Lead/Borated-poly/Lead (Nonalternating)	$2.5x10^{-7}$
Lead/Borated-poly (Nonalternating)	$3x10^{-7}$
Lead/Borated-poly (alternating)	$7.1x10^{-7}$

Table 4. Maximum halo current allowed for various localized shielding models at 75 cm.

D. OPERATIONAL TIME CONSIDERATIONS

The previous models assumed an occupancy and running time of 2000 hr/yr. The operational time of an FEL for communications or other applications could have considerably less operating time than the 2000 hours presented. Radiation limits above were based on the 5 rem/yr federal limits for facility workers. If the same limits were applied to a shorter operational time, then shielding requirements would be reduced. Figure 45 shows the effect on the localized shielding required when operational time is reduced down to 2 hrs/yr. It is important to note that receiving the radiation limit in a short period may raise some concerns. Operation of the FEL in the applications previously mentioned would most likely be shorter segments of time (i.e., seconds to minutes at a time) throughout the year. This would allow for lower administrative radiation exposure limits to be established and ensure higher control of personnel exposure. However, even with the adjustment of operational time, reduction of halo current lost still remains the primary method of reducing the shielding and personnel radiation exposure.

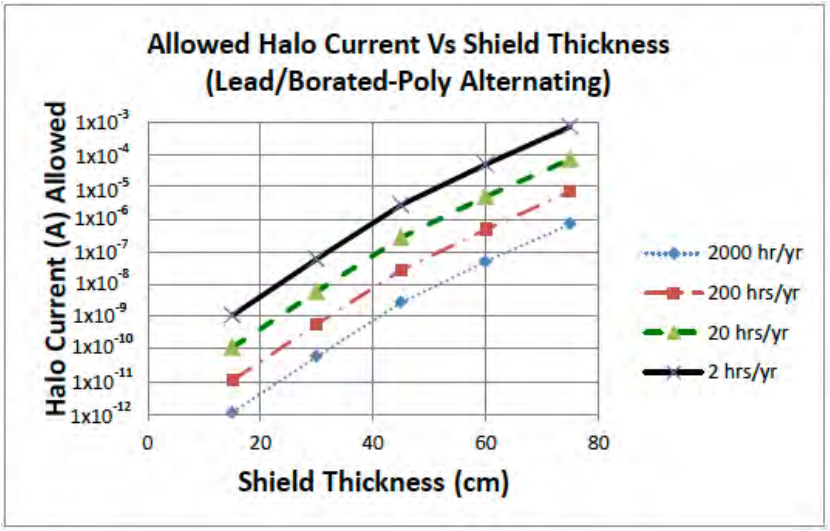

Figure 45. Maximum halo current loss versus shield thickness for lead/borated-poly alternating, with varying operational time.

E. WEIGHT CONSIDERATIONS

The localized shielding models show that is it possible to provide enough shielding for radiation protection of equipment and personnel. Use of heavier materials in the localized shielding may raise concerns of weight issues. Figure 46 shows the relationship between the maximum halo current lost and the amount of shielding weight. The localized shielding can be broken into smaller sections and placed in areas of high halo loss along the FEL beamline, such as pipe bends. This graph assumes a total of 5 meters in length of shielding materials will be used throughout the beamline. The different lines correspond to the varying operational time shown previously in Figure 45.

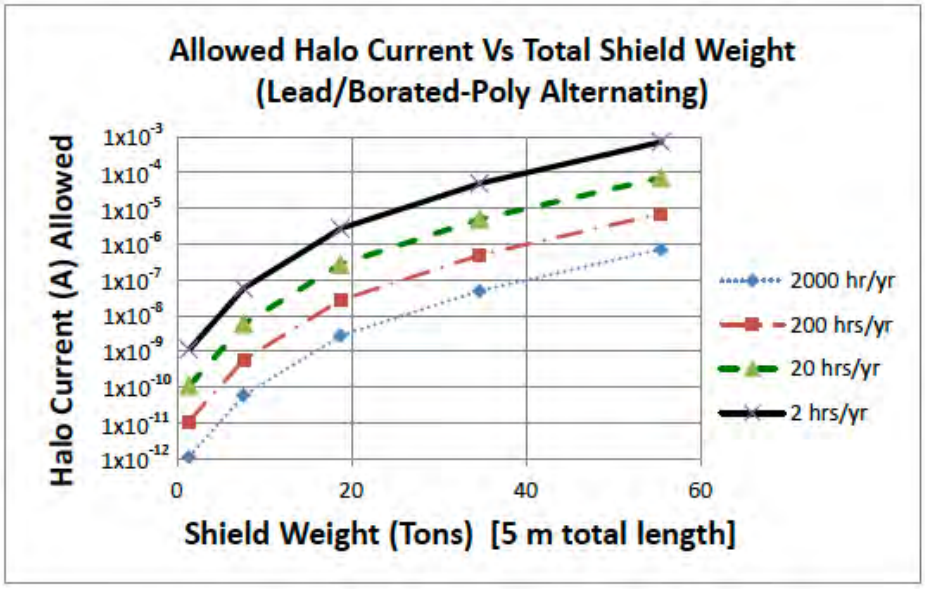

Figure 46. Maximum halo current loss versus shield weight for lead/borated-poly alternating, with varying operational time.

VIII. CONCLUSION

This thesis covered the aspects of operation of the FEL and how halo electrons co-exist with the core electron beam. We also showed that halo electrons with an excessive angle or radial position could collide with the inner surface of the beamline. These collisions could be a radiation hazard and would require shielding in order minimize the hazard for both personnel and equipment.

We showed that the use of a single shielding material is not the most effective method of shielding high energy electrons. In this thesis, we were able to contrast the differences between traditional vault shielding and localized shielding. The results from the different geometries showed that use of localized shielding could reduce or possibly eliminate the requirements of the shielding on the vault walls. This use of localized shielding also showed that with adequate construction, halo current losses up ~1 μA could be supported without exceeding exposure limits. Localized shielding configurations could offer the possibility of mobile designs of an FEL without compromising radiation safety for personnel.

Recommendations for future work are:

- Continue to explore the possible shielding geometries, and materials.
- Examine effects of activation of vault components based on different shielding configurations.
- Examine the shielding requirements of the different ERL FEL designs with applicable monte-carlo software.

THIS PAGE INTENTIONALLY LEFT BLANK

APPENDIX

A. CONCRETE ONLY FLUKA INPUT FILE

```
* D:\Desktop\FLUKA inputs\concrete.dat
* Created: 6.10.2011
* At: 23:59:29
200CM-CONCRETE
MC-CAD Test
GLOBAL      100000.0       0.0       0.0       0.0       1.0
BEAM           -.1       0.0      30.0       .3       0.0      -1.0ELECTRON
BEAMPOS         0.0       0.0      -50.       0.0       0.0
AUXSCORE     USRBIN                    dose      dose         AMB74
USRBIN          11.   DOSE-EQ      -23.      100.       0.0      581.dose
USRBIN          0.0       0.0      551.       50.       36.       30.&
USRBIN          11.     E+&E-      -24.      100.       0.0      581.det-e
USRBIN          0.0       0.0      551.       50.       36.       30.&
USRBIN          11.  EM-ENRGY      -25.      100.       0.0      581.det-em
USRBIN          0.0       0.0      551.       50.       36.       30.&
USRBIN          11.   NEUTRON      -26.      100.       0.0      581.det-n
USRBIN          0.0       0.0      551.       25.       36.       15.&
USRBIN          11.  EM-ENRGY      -21.      270.       0.0      590.det-em
USRBIN          0.0       0.0     -275.      100.       36.      250.&
USRBIN          11.   NEUTRON      -22.      270.       0.0      590.det-n
USRBIN          0.0       0.0     -275.      100.       36.      250.&
START        100000.
PHOTONUC         1.                   LEAD      LEAD
PHOTONUC         1.                Concrete  Concrete
GEOBEGIN                                              COMBNAME
    0    0               MC-CAD
* blkhole
SPH blkhole    0.00 0.00 0.00 100000.00
* conc1
RCC conc1      0.00 0.00 -250. 0.00 0.00 700. 150.
* conc2
RCC conc2      0.00 0.00 -270. 0.00 0.00 740. 170.
* conc3
RCC conc3      0.00 0.00 -290. 0.00 0.00 780. 190.
* conc4
RCC conc4      0.00 0.00 -310. 0.00 0.00 820. 210.
* conc5
RCC conc5      0.00 0.00 -330. 0.00 0.00 860. 230.
* pipe_in
RCC pipe_in    0.00 0.00 -100.25 0.00 0.00 400. 2.25
* pipe_out
RCC pipe_out   0.00 0.00 -100.5 0.00 0.00 400.5 2.50
* void
SPH void       0.00 0.00 0.00 10000.00
RCC det1       0.0 0.0 551. 0.0 0.0 10. 100.
RCC det2       0.0 0.0 561. 0.0 0.0 10. 100.
```

```
RCC det3       0.0 0.0 571. 0.0 0.0 10. 100.
RCC chamber5   0.0 0.0 -230. 0.0 0.0 660. 130.
RCC chamber4   0.0 0.0 -210. 0.0 0.0 620. 110.
RCC chamber3   0.0 0.0 -190. 0.0 0.0 580. 90.
RCC chamber2   0.0 0.0 -170. 0.0 0.0 540. 70.
RCC chamber1   0.0 0.0 -150. 0.0 0.0 500. 50.
RCC conc6      0.0 0.0 -350. 0.0 0.0 900. 250.
END
* BLACKHOLE REGION OUTSIDE VOID
BLKHOLE      5 +blkhole  -void
* PIPE
PIPE         5 +pipe_out  -pipe_in
CHAMBER1     5 +chamber2 -chamber1
CHAMBER2     5 +chamber3 -chamber2
CHAMBER3     5 +chamber4 -chamber3
CHAMBER4     5 +chamber5 -chamber4
CHAMBER5     5 +conc1   -chamber5
* VAULT
VAULT        5 +chamber1 -pipe_out
* INSIDE THE BEAM PIPE
BMLINE       5 +pipe_in
* VOID REGION OUTSIDE WALL
VOID         5 +void -conc6 -det1 -det2 -det3
* 1ST 5CM OF WATER DETECTOR
DET1         5 +det1 -det2
* 2ND 5CM WATER DETECTOR
DET2         5 +det2 -det3
* 3RD 5CM OF WATER DETECTOR
DET3         5 +det3
CONC1        5 +conc2  -conc1
CONC2        5 +conc3  -conc2
CONC3        5 +conc4  -conc3
CONC4        5 +conc5  -conc4
CONC5        5 +conc6  -conc5
END
GEOEND
ASSIGNMA      WATER     DET1
ASSIGNMA      WATER     DET2
ASSIGNMA      WATER     DET3
* Concrete
* Concrete has a wide variation in density and composition. The above
* description is for poured structural concrete with 10% moisture
* content. Concrete block will have a density of about 2.05 g/cm3.
* Ranges of concrete composition are : C (8–25%), O (38–60%), Si (8–18%).
* Concrete composition can be analyzed cheaply by commercial laboratories.
MATERIAL                      2.34                       Concrete
COMPOUND       23.0   CARBON      40.0   OXYGEN      12.0   SILICONConcrete
COMPOUND       12.0   CALCIUM     10.0  HYDROGEN       2.0  MAGNESIUConcrete
MATERIAL        24.   51.9961     7.18                       CHROMIUM
* Stainless-Steel (typical)
* Stainless-Steel is produced with Cr content ranging from
* 4 - 19 Atomic Percent, and with C content from 0 - 4 percent.
```

```
MATERIAL                  8.0                     Stainles
COMPOUND      18.0 CHROMIUM     74.0     IRON      8.0    NICKELStainles
ASSIGNMA   BLCKHOLE   BLKHOLE
ASSIGNMA   Stainles      PIPE
ASSIGNMA        AIR     VAULT
ASSIGNMA   Concrete  CHAMBER1
ASSIGNMA   Concrete  CHAMBER2
ASSIGNMA   Concrete  CHAMBER3
ASSIGNMA   Concrete  CHAMBER4
ASSIGNMA   Concrete  CHAMBER5
ASSIGNMA     VACUUM    BMLINE
ASSIGNMA     VACUUM      VOID
ASSIGNMA   Concrete     CONC1
ASSIGNMA   Concrete     CONC1
ASSIGNMA   Concrete     CONC2
ASSIGNMA   Concrete     CONC3
ASSIGNMA   Concrete     CONC4
ASSIGNMA   Concrete     CONC5
BIASING        0.0       1.    .0001    BMLINE
BIASING        0.0       1.    .0002     PIPE
BIASING        0.0       1.    .0002     VAULT
BIASING        0.0       1.  114.688      DET1
BIASING        0.0       1.    1026.      DET2
BIASING        0.0       1.    9234.      DET3
BIASING        0.0      1.0    .0008   CHAMBER1
BIASING        0.0      1.0    .0008   CHAMBER2
BIASING        0.0      1.0    .0032   CHAMBER3
BIASING        0.0      1.0    .0032   CHAMBER4
BIASING        0.0      1.0    .0128   CHAMBER5
BIASING        0.0      1.0    .0128     CONC1
BIASING        0.0      1.0     .512     CONC2
BIASING        0.0      1.0    1.024     CONC3
BIASING        0.0      1.0    4.096     CONC4
BIASING        0.0      1.0   16.384     CONC5
BIASING        0.0      1.0   16.384      VOID
STOP
```

B. LEAD-CONCRETE FLUKA INPUT FILE

```
* D:\Desktop\FLUKA inputs\pbconcrete.dat
* Created: 6.10.2011
* At: 23:59:29
PB-CONCRETE
MC-CAD Test
GLOBAL       1000.0       0.0       0.0       0.0       1.0
BEAM           -.1       0.0      30.0       .3       0.0      -1.0ELECTRON
BEAMPOS         0.0       0.0      -50.      0.0       0.0
AUXSCORE     USRBIN                    dose      dose         AMB74
USRBIN         11.   DOSE-EQ     -23.      100.      0.0      581.dose
USRBIN         0.0       0.0      551.      50.       36.       30.&
USRBIN         11.    E+&E-      -24.      100.      0.0      581.det-e
USRBIN         0.0       0.0      551.      50.       36.       30.&
```

```
USRBIN         11.  EM-ENRGY     -25.      100.       0.0      581.det-em
USRBIN         0.0       0.0      551.       50.       36.       30.&
USRBIN         11.   NEUTRON     -26.      100.       0.0      581.det-n
USRBIN         0.0       0.0      551.       25.       36.       15.&
USRBIN         11.  EM-ENRGY     -21.      260.       0.0      590.det-em
USRBIN         0.0       0.0    -275.      100.       36.      250.&
USRBIN         11.   NEUTRON     -22.      260.       0.0      590.det-n
USRBIN         0.0       0.0    -275.      100.       36.      250.&
START       200000.
PHOTONUC        1.                  LEAD     LEAD
PHOTONUC        1.                Concrete  Concrete
GEOBEGIN                                              COMBNAME
    0    0               MC-CAD
* blkhole
SPH blkhole    0.00 0.00 0.00 100000.00
* conc1
RCC conc1      0.00 0.00 -250. 0.00 0.00 700. 150.
* conc2
RCC conc2      0.00 0.00 -270. 0.00 0.00 740. 170.
* conc3
RCC conc3      0.00 0.00 -290. 0.00 0.00 780. 190.
* conc4
RCC conc4      0.00 0.00 -310. 0.00 0.00 820. 210.
* conc5
RCC conc5      0.00 0.00 -330. 0.00 0.00 860. 230.
* pipe_in
RCC pipe_in    0.00 0.00 -100.25 0.00 0.00 400. 2.25
* pipe_out
RCC pipe_out   0.00 0.00 -100.5 0.00 0.00 400.5 2.50
* void
SPH void       0.00 0.00 0.00 10000.00
RCC det1       0.0 0.0 551. 0.0 0.0 10. 100.
RCC det2       0.0 0.0 561. 0.0 0.0 10. 100.
RCC det3       0.0 0.0 571. 0.0 0.0 10. 100.
RCC chamber5   0.0 0.0 -250. 0.0 0.0 697. 150.
RCC chamber4   0.0 0.0 -250. 0.0 0.0 694. 150.
RCC chamber3   0.0 0.0 -250. 0.0 0.0 691. 150.
RCC chamber2   0.0 0.0 -250. 0.0 0.0 688. 150.
RCC chamber1   0.0 0.0 -250. 0.0 0.0 685. 150.
RCC conc6      0.0 0.0 -350. 0.0 0.0 900. 250.
END
* BLACKHOLE
BLKHOLE      5 +blkhole  -void
* PIPE
PIPE         5 +pipe_out  -pipe_in
CHAMBER1     5 +chamber2 -chamber1
CHAMBER2     5 +chamber3 -chamber2
CHAMBER3     5 +chamber4 -chamber3
CHAMBER4     5 +chamber5 -chamber4
CHAMBER5     5 +conc1    -chamber5
* VAULT
VAULT        5 +chamber1 -pipe_out
```

```
* INSIDE BEAM PIPE
BMLINE      5 +pipe_in
* VOID REGION OUTSIDE WALL
VOID        5 +void -conc6 -det1 -det2 -det3
* 1ST 5CM OF WATER DETECTOR
DET1        5 +det1 -det2
* 2ND 5CM OF WATER DETECTOR
DET2        5 +det2 -det3
* 3RD 5CM OF WATER DETECTOR
DET3        5 +det3
CONC1       5 +conc2  -conc1
CONC2       5 +conc3  -conc2
CONC3       5 +conc4  -conc3
CONC4       5 +conc5  -conc4
CONC5       5 +conc6  -conc5
END
GEOEND
ASSIGNMA      WATER     DET1
ASSIGNMA      WATER     DET2
ASSIGNMA      WATER     DET3
* Concrete
* Concrete has a wide variation in density and composition. The above
* description is for poured structural concrete with 10% moisture
* content. Concrete block will have a density of about 2.05 g/cm3.
* Ranges of concrete composition are : C (8–25%), O (38–60%), Si (8–18%).
* Concrete composition can be analyzed cheaply by commercial laboratories.
MATERIAL                    2.34                    Concrete
COMPOUND       23.0   CARBON      40.0   OXYGEN      12.0   SILICONConcrete
COMPOUND       12.0   CALCIUM     10.0  HYDROGEN       2.0  MAGNESIUConcrete
MATERIAL        24.   51.9961     7.18                    CHROMIUM
* Stainless-Steel (typical)
* Stainless-Steel is produced with Cr content ranging from
* 4 - 19 Atomic Percent, and with C content from 0 - 4 percent.
MATERIAL                    8.0                     Stainles
COMPOUND       18.0  CHROMIUM     74.0      IRON       8.0    NICKELStainles
ASSIGNMA    BLCKHOLE   BLKHOLE
ASSIGNMA    Stainles      PIPE
ASSIGNMA       AIR     VAULT
ASSIGNMA      LEAD  CHAMBER1
ASSIGNMA      LEAD  CHAMBER2
ASSIGNMA      LEAD  CHAMBER3
ASSIGNMA      LEAD  CHAMBER4
ASSIGNMA      LEAD  CHAMBER5
ASSIGNMA     VACUUM    BMLINE
ASSIGNMA     VACUUM      VOID
ASSIGNMA    Concrete     CONC1
ASSIGNMA    Concrete     CONC1
ASSIGNMA    Concrete     CONC2
ASSIGNMA    Concrete     CONC3
ASSIGNMA    Concrete     CONC4
ASSIGNMA    Concrete     CONC5
BIASING        0.0       1.    .00025    BMLINE
```

```
BIASING         0.0       1.    .00025      PIPE
BIASING         0.0       1.    .00025     VAULT
BIASING         0.0       1.   524.288       DET1
BIASING         0.0       1.   1310.72       DET2
BIASING         0.0       1.   3932.16       DET3
BIASING         0.0      1.0      .001  CHAMBER1
BIASING         0.0      1.0      .004  CHAMBER2
BIASING         0.0      1.0      .016  CHAMBER3
BIASING         0.0      1.0      .064  CHAMBER4
BIASING         0.0      1.0      .256  CHAMBER5
BIASING         0.0      1.0     1.024     CONC1
BIASING         0.0      1.0     4.096     CONC2
BIASING         0.0      1.0    16.384     CONC3
BIASING         0.0      1.0    65.536     CONC4
BIASING         0.0      1.0   262.144     CONC5
BIASING         0.0      1.0   262.144      VOID
STOP
```

C. LOCALIZED BORATED-POLY AND LEAD ALTERNATING

```
* D:\Desktop\FLUKA inputs\bplypbalt.dat
* Created: 6.10.2011
* At: 23:59:29
BPLY-PB-ALTX5
MC-CAD Test
GLOBAL       1000.0       0.0       0.0       0.0       1.0
BEAM           -.1       0.0      30.0       .3       0.0      -1.0ELECTRON
BEAMPOS         0.0       0.0      -50.      0.0       0.0
AUXSCORE     USRBIN                      dose      dose         AMB74
USRBIN          11.   DOSE-EQ      -23.       50.       0.0   481.635dose
USRBIN          0.0       0.0   451.635       50.       36.       30.&
USRBIN          11.   DOSE-EQ      -27.   161.635       0.0      330.dose$
USRBIN       131.635       0.0      230.       50.       36.       30.&
USRBIN          11.    E+&E-      -24.       50.       0.0   481.635det-e
USRBIN          0.0       0.0   451.635       50.       36.       30.&
USRBIN          11.  EM-ENRGY      -25.       50.       0.0   481.635det-em
USRBIN          0.0       0.0   451.635       50.       36.       30.&
USRBIN          11.   NEUTRON      -26.       50.       0.0   481.635det-n
USRBIN          0.0       0.0   451.635       25.       36.       15.&
USRBIN          11.  EM-ENRGY      -21.      180.       0.0      490.det-em
USRBIN          0.0       0.0     -275.      100.       36.      250.&
USRBIN          11.   NEUTRON      -22.      180.       0.0      490.det-n
USRBIN          0.0       0.0     -275.      100.       36.      250.&
START        100000.
PHOTONUC         1.                    LEAD
PHOTONUC         1.                  POLYETHY
PHOTONUC        0.0                    WATER
GEOBEGIN                                                COMBNAME
    0    0               MC-CAD
* blkhole
SPH blkhole    0.00 0.00 0.00 100000.00
* out_blkhd
```

```
RCC outblkhd   0.00 0.00 -250.635 0.00 0.00 701.27 130.635
* in_blkhd
RCC in_blkhd   0.00 0.00 -250. 0.00 0.00 700. 130.
* pipe_in
RCC pipe_in    0.00 0.00 -99.75 0.00 0.00 400. 2.25
* pipe_out
RCC pipe_out   0.00 0.00 -100. 0.00 0.00 400.5 2.50
* void
SPH void       0.00 0.00 0.00 10000.00
RCC det1_1     0.0 0.0 451.635 0.0 0.0 10. 50.
RCC det1_2     0.0 0.0 461.635 0.0 0.0 10. 50.
RCC det1_3     0.0 0.0 471.635 0.0 0.0 10. 50.
RCC det2_1     0.0 0.0 230. 0.0 0.0 100. 131.635
RCC det2_2     0.0 0.0 230. 0.0 0.0 100. 141.635
RCC det2_3     0.0 0.0 230. 0.0 0.0 100. 151.635
RCC det2_4     0.0 0.0 230. 0.0 0.0 100. 161.635
RCC extra1     0.0 0.0 -100. 0.0 0.0 468. 70.
RCC extra2     0.0 0.0 -100. 0.0 0.0 475.5 77.5
RCC poly4      0.0 0.0 -100. 0.0 0.0 460.5 62.5
RCC poly3      0.0 0.0 -100. 0.0 0.0 453. 55.
RCC poly2      0.0 0.0 -100. 0.0 0.0 445.5 47.5
RCC poly1      0.0 0.0 -100. 0.0 0.0 438. 40.
RCC pb4        0.0 0.0 -100. 0.0 0.0 430.5 32.5
RCC pb3        0.0 0.0 -100. 0.0 0.0 423. 25.
RCC pb2        0.0 0.0 -100. 0.0 0.0 415.5 17.5
RCC pb1        0.0 0.0 -100. 0.0 0.0 408. 10.
END
* Blackhole outside void
BLKHOLE      5 +blkhole  -void
* Pipe
PIPE         5 +pipe_out  -pipe_in
PB1          5 +pb1 -pipe_out
PB2          5 +pb2 -pb1
PB3          5 +pb3 -pb2
PB4          5 +pb4 -pb3
extra1       5 +extra1 -poly4
extra2       5 +extra2 -extra1
* Vault
VAULT        5 +in_blkhd -extra2
* INSIDE BEAMPIPE
BMLINE       5 +pipe_in
* VOID AREA OUTSIDE TRAILER
VOID         5 +void -outblkhd  -det1_1 -det1_2 -det1_3 -det2_1 -det2_2 -det2_3 -det2_4
* 1ST 5CM OF WATER DETECTOR
DET1_1       5 +det1_1
* 2ND 5CM OF WATER DETECTOR
DET1_2       5 +det1_2
* 3RD 5CM OF WATER DETECTOR
DET1_3       5 +det1_3
* 1ST 5CM OF WATER DETECTOR
DET2_1       5 +det2_2 -det2_1
* 2ND 5CM OF WATER DETECTOR
```

```
DET2_2       5 +det2_3 -det2_2
* 3RD 5CM OF WATER DETECTOR
DET2_3       5 +det2_4 -det2_3
* WALL OF TRAILER
BLKHD        5 +outblkhd -in_blkhd
* AIRGAP BETWEEN SIDE DETECTOR AND WALL
AIRGAP       5 -outblkhd +det2_1
POLY1        5 +poly1 -pb4
POLY2        5 +poly2 -poly1
POLY3        5 +poly3 -poly2
POLY4        5 +poly4 -poly3
END
GEOEND
ASSIGNMA      WATER    DET1_1
ASSIGNMA      WATER    DET1_2
ASSIGNMA      WATER    DET1_3
ASSIGNMA      WATER    DET2_1
ASSIGNMA      WATER    DET2_2
ASSIGNMA      WATER    DET2_3
ASSIGNMA     VACUUM    AIRGAP
* Concrete
* Concrete has a wide variation in density and composition. The above
* description is for poured structural concrete with 10% moisture
* content. Concrete block will have a density of about 2.05 g/cm3.
* Ranges of concrete composition are : C (8–25%), O (38–60%), Si (8–18%).
* Concrete composition can be analyzed cheaply by commercial laboratories.
MATERIAL                    2.34                    Concrete
COMPOUND      23.0    CARBON     40.0    OXYGEN     12.0   SILICONConcrete
COMPOUND      12.0   CALCIUM     10.0  HYDROGEN      2.0  MAGNESIUConcrete
MATERIAL        24.   51.9961     7.18                    CHROMIUM
* Stainless-Steel (typical)
* Stainless-Steel is produced with Cr content ranging from
* 4 - 19 Atomic Percent, and with C content from 0 - 4 percent.
MATERIAL                    8.0                     Stainles
COMPOUND      18.0  CHROMIUM     74.0     IRON       8.0    NICKELStainles
MATERIAL        5.    10.811     2.34                    BORON
* Boron-Poly
* SWX-210
MATERIAL                    1.12                    Boron-po
COMPOUND      -8.54  HYDROGEN    -30.0     BORON    -59.25    CARBONBoron-po
COMPOUND       -.76    OXYGEN    -1.01   SILICON     -0.38      IRONBoron-po
ASSIGNMA    BLCKHOLE   BLKHOLE
ASSIGNMA    Stainles      PIPE
ASSIGNMA         AIR     VAULT
ASSIGNMA    Boron-po       PB1
ASSIGNMA        LEAD       PB2
ASSIGNMA    Boron-po       PB3
ASSIGNMA        LEAD       PB4
ASSIGNMA     VACUUM    BMLINE
ASSIGNMA     VACUUM      VOID
ASSIGNMA    Boron-po     POLY1
ASSIGNMA        LEAD     POLY2
```

```
ASSIGNMA    Boron-po     POLY3
ASSIGNMA        LEAD     POLY4
ASSIGNMA    Boron-po    extra1
ASSIGNMA        LEAD    extra2
ASSIGNMA    Stainles     BLKHD
BIASING         0.0        1.     .0001    BMLINE
BIASING         0.0        1.     .0001     PIPE
BIASING         0.0        1.     .0005      PB1
BIASING         0.0        1.     .0025      PB2
BIASING         0.0        1.     .0125      PB3
BIASING         0.0        1.     .0625      PB4
BIASING         0.0       1.0     .3125     POLY1
BIASING         0.0       1.0    1.5625     POLY2
BIASING         0.0       1.0    7.8125     POLY3
BIASING         0.0       1.0   39.0625      POLY4
BIASING         0.0       1.0   195.313     extra1
BIASING         0.0       1.0   976.563     extra2
BIASING         0.0       1.0   976.563      VAULT
BIASING         0.0       1.0   976.563      BLKHD
BIASING         0.0        1.   976.563     AIRGAP
BIASING         0.0        1.   976.563      VOID
BIASING         0.0       1.0   1953.13     DET1_1
BIASING         0.0       1.0   3906.25     DET1_2
BIASING         0.0       1.0    7812.5     DET1_3
BIASING         0.0       1.0   1953.13     DET2_1
BIASING         0.0       1.0   3906.25     DET2_2
BIASING         0.0       1.0    7812.5     DET2_3
STOP
```

D. LOCALIZED LEAD AND BORATED-POLY ALTERNATING

```
* D:\Desktop\FLUKA inputs\pbbplyalt.dat
* Created: 6.10.2011
* At: 23:59:29
PB-BPLY-ALTX5
MC-CAD Test
GLOBAL       1000.0       0.0       0.0       0.0       1.0
BEAM           -.1       0.0      30.0       .3       0.0      -1.0ELECTRON
BEAMPOS         0.0       0.0      -50.       0.0       0.0
AUXSCORE     USRBIN                    dose      dose         AMB74
USRBIN          11.   DOSE-EQ      -23.       50.       0.0   481.635dose
USRBIN          0.0       0.0   451.635       50.       36.       30.&
USRBIN          11.   DOSE-EQ      -27.   161.635       0.0      330.dose$
USRBIN       131.635       0.0      230.       50.       36.       30.&
USRBIN          11.     E+&E-      -24.       50.       0.0   481.635det-e
USRBIN          0.0       0.0   451.635       50.       36.       30.&
USRBIN          11.  EM-ENRGY      -25.       50.       0.0   481.635det-em
USRBIN          0.0       0.0   451.635       50.       36.       30.&
USRBIN          11.   NEUTRON      -26.       50.       0.0   481.635det-n
USRBIN          0.0       0.0   451.635       25.       36.       15.&
USRBIN          11.  EM-ENRGY      -21.      180.       0.0      490.det-em
USRBIN          0.0       0.0     -275.      100.       36.      250.&
```

```
USRBIN         11.   NEUTRON     -22.      180.       0.0      490.det-n
USRBIN         0.0       0.0     -275.      100.       36.      250.&
START       100000.
PHOTONUC        1.                    LEAD
PHOTONUC        1.                 POLYETHY
PHOTONUC       0.0                    WATER
GEOBEGIN                                                  COMBNAME
   0    0                MC-CAD
* blkhole
SPH blkhole    0.00 0.00 0.00 100000.00
* out_blkhd
RCC outblkhd   0.00 0.00 -250.635 0.00 0.00 701.27 130.635
* in_blkhd
RCC in_blkhd   0.00 0.00 -250. 0.00 0.00 700. 130.
* pipe_in
RCC pipe_in    0.00 0.00 -99.75 0.00 0.00 400. 2.25
* pipe_out
RCC pipe_out   0.00 0.00 -100. 0.00 0.00 400.5 2.50
* void
SPH void       0.00 0.00 0.00 10000.00
RCC det1_1     0.0 0.0 451.635 0.0 0.0 10. 50.
RCC det1_2     0.0 0.0 461.635 0.0 0.0 10. 50.
RCC det1_3     0.0 0.0 471.635 0.0 0.0 10. 50.
RCC det2_1     0.0 0.0 230. 0.0 0.0 100. 131.635
RCC det2_2     0.0 0.0 230. 0.0 0.0 100. 141.635
RCC det2_3     0.0 0.0 230. 0.0 0.0 100. 151.635
RCC det2_4     0.0 0.0 230. 0.0 0.0 100. 161.635
RCC extra1     0.0 0.0 -100. 0.0 0.0 468. 70.
RCC extra2     0.0 0.0 -100. 0.0 0.0 475.5 77.5
RCC poly4      0.0 0.0 -100. 0.0 0.0 460.5 62.5
RCC poly3      0.0 0.0 -100. 0.0 0.0 453. 55.
RCC poly2      0.0 0.0 -100. 0.0 0.0 445.5 47.5
RCC poly1      0.0 0.0 -100. 0.0 0.0 438. 40.
RCC pb4        0.0 0.0 -100. 0.0 0.0 430.5 32.5
RCC pb3        0.0 0.0 -100. 0.0 0.0 423. 25.
RCC pb2        0.0 0.0 -100. 0.0 0.0 415.5 17.5
RCC pb1        0.0 0.0 -100. 0.0 0.0 408. 10.
END
* BLACKHOLE OUTSIDE OF VOID
BLKHOLE      5 +blkhole  -void
* PIPE
PIPE         5 +pipe_out  -pipe_in
PB1          5 +pb1 -pipe_out
PB2          5 +pb2 -pb1
PB3          5 +pb3 -pb2
PB4          5 +pb4 -pb3
extra1       5 +extra1 -poly4
extra2       5 +extra2 -extra1
* VAULT
VAULT        5 +in_blkhd -extra2
* INSIDE PIPE
BMLINE       5 +pipe_in
```

```
* VOID AREA OUTSIDE TRAILER
VOID         5 +void -outblkhd  -det1_1 -det1_2 -det1_3 -det2_1 -det2_2 -det2_3 -det2_4
* 1ST 5CM OF WATER DETECTOR
DET1_1       5 +det1_1
* 2ND 5CM OF WATER DETECTOR
DET1_2       5 +det1_2
* 3RD 5CM OF WATER DETECTOR
DET1_3       5 +det1_3
* 1ST 5CM OF WATER DETECTOR
DET2_1       5 +det2_2 -det2_1
* 2ND 5CM OF WATER DETECTOR
DET2_2       5 +det2_3 -det2_2
* 3RD 5CM OF WATER DETECTOR
DET2_3       5 +det2_4 -det2_3
* WALL OF TRAILER
BLKHD        5 +outblkhd -in_blkhd
* AIRGAP BETWEEN SIDE DETECTOR AND WALL
AIRGAP       5 -outblkhd +det2_1
POLY1        5 +poly1 -pb4
POLY2        5 +poly2 -poly1
POLY3        5 +poly3 -poly2
POLY4        5 +poly4 -poly3
END
GEOEND
ASSIGNMA      WATER    DET1_1
ASSIGNMA      WATER    DET1_2
ASSIGNMA      WATER    DET1_3
ASSIGNMA      WATER    DET2_1
ASSIGNMA      WATER    DET2_2
ASSIGNMA      WATER    DET2_3
ASSIGNMA     VACUUM    AIRGAP
* Concrete
* Concrete has a wide variation in density and composition. The above
* description is for poured structural concrete with 10% moisture
* content. Concrete block will have a density of about 2.05 g/cm3.
* Ranges of concrete composition are : C (8–25%), O (38–60%), Si (8–18%).
* Concrete composition can be analyzed cheaply by commercial laboratories.
MATERIAL                      2.34                       Concrete
COMPOUND       23.0    CARBON      40.0    OXYGEN      12.0   SILICONConcrete
COMPOUND       12.0   CALCIUM      10.0  HYDROGEN       2.0  MAGNESIUConcrete
MATERIAL        24.   51.9961      7.18                      CHROMIUM
* Stainless-Steel (typical)
* Stainless-Steel is produced with Cr content ranging from
* 4 - 19 Atomic Percent, and with C content from 0 - 4 percent.
MATERIAL                      8.0                        Stainles
COMPOUND       18.0  CHROMIUM      74.0      IRON       8.0    NICKELStainles
MATERIAL         5.    10.811      2.34                    BORON
* Boron-Poly
* SWX-210
MATERIAL                      1.12                       Boron-po
COMPOUND      -8.54  HYDROGEN     -30.0     BORON     -59.25    CARBONBoron-po
COMPOUND       -.76    OXYGEN     -1.01    SILICON     -0.38      IRONBoron-po
```

```
ASSIGNMA    BLCKHOLE   BLKHOLE
ASSIGNMA    Stainles      PIPE
ASSIGNMA         AIR     VAULT
ASSIGNMA        LEAD       PB1
ASSIGNMA    Boron-po       PB2
ASSIGNMA        LEAD       PB3
ASSIGNMA    Boron-po       PB4
ASSIGNMA      VACUUM    BMLINE
ASSIGNMA      VACUUM      VOID
ASSIGNMA        LEAD     POLY1
ASSIGNMA    Boron-po     POLY2
ASSIGNMA        LEAD     POLY3
ASSIGNMA    Boron-po     POLY4
ASSIGNMA        LEAD    extra1
ASSIGNMA    Boron-po    extra2
ASSIGNMA    Stainles     BLKHD
BIASING         0.0        1.     .0001    BMLINE
BIASING         0.0        1.     .0001      PIPE
BIASING         0.0        1.     .0005       PB1
BIASING         0.0        1.     .0025       PB2
BIASING         0.0        1.     .0125       PB3
BIASING         0.0        1.     .0625       PB4
BIASING         0.0       1.0      .3125     POLY1
BIASING         0.0       1.0     1.5625     POLY2
BIASING         0.0       1.0     7.8125     POLY3
BIASING         0.0       1.0    39.0625      POLY4
BIASING         0.0       1.0    195.313     extra1
BIASING         0.0       1.0    976.563     extra2
BIASING         0.0       1.0    976.563      VAULT
BIASING         0.0       1.0    976.563      BLKHD
BIASING         0.0        1.    976.563     AIRGAP
BIASING         0.0        1.    976.563      VOID
BIASING         0.0       1.0    1953.13     DET1_1
BIASING         0.0       1.0    3906.25     DET1_2
BIASING         0.0       1.0     7812.5     DET1_3
BIASING         0.0       1.0    1953.13     DET2_1
BIASING         0.0       1.0    3906.25     DET2_2
BIASING         0.0       1.0     7812.5     DET2_3
STOP
```

E. LOCALIZED LEAD AND BORATED-POLY NONALTERNATING

```
* D:\Desktop\FLUKA inputs\pbbplynonalt.dat
* Created: 6.10.2011
* At: 23:59:29
PB-BPLY-NONALT
MC-CAD Test
GLOBAL       1000.0       0.0       0.0       0.0       1.0
BEAM           -.1       0.0      30.0       .3       0.0      -1.0ELECTRON
BEAMPOS         0.0       0.0      -50.       0.0       0.0
AUXSCORE     USRBIN                      dose      dose         AMB74
USRBIN         11.   DOSE-EQ      -23.       50.       0.0   481.635dose
```

```
USRBIN          0.0       0.0   451.635       50.       36.       30.&
USRBIN          11.   DOSE-EQ      -27.   161.635       0.0      330.dose$
USRBIN       131.635       0.0      230.       50.       36.       30.&
USRBIN          11.     E+&E-      -24.       50.       0.0   481.635det-e
USRBIN          0.0       0.0   451.635       50.       36.       30.&
USRBIN          11.  EM-ENRGY      -25.       50.       0.0   481.635det-em
USRBIN          0.0       0.0   451.635       50.       36.       30.&
USRBIN          11.   NEUTRON      -26.       50.       0.0   481.635det-n
USRBIN          0.0       0.0   451.635       25.       36.       15.&
USRBIN          11.  EM-ENRGY      -21.      180.       0.0      490.det-em
USRBIN          0.0       0.0    -275.      100.       36.      250.&
USRBIN          11.   NEUTRON      -22.      180.       0.0      490.det-n
USRBIN          0.0       0.0    -275.      100.       36.      250.&
START        100000.
PHOTONUC         1.                    LEAD
PHOTONUC         1.                  POLYETHY
PHOTONUC        0.0                    WATER
GEOBEGIN                                                COMBNAME
    0    0               MC-CAD
* blkhole
SPH blkhole    0.00 0.00 0.00 100000.00
* out_blkhd
RCC outblkhd   0.00 0.00 -250.635 0.00 0.00 701.27 130.635
* in_blkhd
RCC in_blkhd   0.00 0.00 -250. 0.00 0.00 700. 130.
* pipe_in
RCC pipe_in    0.00 0.00 -99.75 0.00 0.00 400. 2.25
* pipe_out
RCC pipe_out   0.00 0.00 -100. 0.00 0.00 400.5 2.50
* void
SPH void       0.00 0.00 0.00 10000.00
RCC det1_1     0.0 0.0 451.635 0.0 0.0 10. 50.
RCC det1_2     0.0 0.0 461.635 0.0 0.0 10. 50.
RCC det1_3     0.0 0.0 471.635 0.0 0.0 10. 50.
RCC det2_1     0.0 0.0 230. 0.0 0.0 100. 131.635
RCC det2_2     0.0 0.0 230. 0.0 0.0 100. 141.635
RCC det2_3     0.0 0.0 230. 0.0 0.0 100. 151.635
RCC det2_4     0.0 0.0 230. 0.0 0.0 100. 161.635
RCC poly4      0.0 0.0 -100. 0.0 0.0 468. 70.
RCC poly5      0.0 0.0 -100. 0.0 0.0 475.5 77.5
RCC poly3      0.0 0.0 -100. 0.0 0.0 460.5 62.5
RCC poly2      0.0 0.0 -100. 0.0 0.0 453. 55.
RCC poly1      0.0 0.0 -100. 0.0 0.0 445.5 47.5
RCC pb5        0.0 0.0 -100. 0.0 0.0 438. 40.
RCC pb4        0.0 0.0 -100. 0.0 0.0 430.5 32.5
RCC pb3        0.0 0.0 -100. 0.0 0.0 423. 25.
RCC pb2        0.0 0.0 -100. 0.0 0.0 415.5 17.5
RCC pb1        0.0 0.0 -100. 0.0 0.0 408. 10.
END
* BLACKHOLE REGION OUTSIDE VOID
BLKHOLE      5 +blkhole  -void
PIPE         5 +pipe_out  -pipe_in
```

```
PB1         5 +pb1 -pipe_out
PB2         5 +pb2 -pb1
PB3         5 +pb3 -pb2
PB4         5 +pb4 -pb3
POLY4       5 +poly4 -poly3
POLY5       5 +poly5 -poly4
* VAULT;
VAULT       5 +in_blkhd -poly5
* BEAMLINE
BMLINE      5 +pipe_in
* OUTSIDE VOID
VOID        5 +void -outblkhd  -det1_1 -det1_2 -det1_3 -det2_1 -det2_2 -det2_3 -det2_4
* FIRST 5CM OF WATER DETECTOR
DET1_1      5 +det1_1
* 2ND 5CM OF WATER DETECTOR
DET1_2      5 +det1_2
* 3RD 5CM OF WATER DETECTOR
DET1_3      5 +det1_3
* 1ST 5CM OF WATER DETECTOR
DET2_1      5 +det2_2 -det2_1
* 2ND 5CM OF WATER DETECTOR
DET2_2      5 +det2_3 -det2_2
* 3RD 5CM OF WATER DETECTOR
DET2_3      5 +det2_4 -det2_3
* OUTER TRAILER WALL
BLKHD       5 +outblkhd -in_blkhd
* 1CM AIRGAP BETWEEN DETECTOR 2 AND THE WALL
AIRGAP      5 -outblkhd +det2_1
PB5         5 +pb5 -pb4
POLY1       5 +poly1 -pb5
POLY2       5 +poly2 -poly1
POLY3       5 +poly3 -poly2
END
GEOEND
ASSIGNMA      WATER    DET1_1
ASSIGNMA      WATER    DET1_2
ASSIGNMA      WATER    DET1_3
ASSIGNMA      WATER    DET2_1
ASSIGNMA      WATER    DET2_2
ASSIGNMA      WATER    DET2_3
ASSIGNMA     VACUUM    AIRGAP
* Concrete
* Concrete has a wide variation in density and composition. The above
* description is for poured structural concrete with 10% moisture
* content. Concrete block will have a density of about 2.05 g/cm3.
* Ranges of concrete composition are : C (8–25%), O (38–60%), Si (8–18%).
* Concrete composition can be analyzed cheaply by commercial laboratories.
MATERIAL                    2.34                        Concrete
COMPOUND       23.0   CARBON      40.0   OXYGEN      12.0   SILICONConcrete
COMPOUND       12.0   CALCIUM     10.0   HYDROGEN     2.0   MAGNESIUConcrete
MATERIAL       24.    51.9961     7.18                       CHROMIUM
* Stainless-Steel (typical)
```

```
* Stainless-Steel is produced with Cr content ranging from
* 4 - 19 Atomic Percent, and with C content from 0 - 4 percent.
MATERIAL                    8.0                     Stainles
COMPOUND      18.0 CHROMIUM     74.0     IRON      8.0   NICKELStainles
MATERIAL        5.   10.811     2.34                BORON
* Boron-Poly
* SWX-210
MATERIAL                    1.12                    Boron-po
COMPOUND     -8.54 HYDROGEN    -30.0    BORON    -59.25   CARBONBoron-po
COMPOUND      -.76 OXYGEN     -1.01   SILICON    -0.38     IRONBoron-po
ASSIGNMA   BLCKHOLE  BLKHOLE
ASSIGNMA   Stainles     PIPE
ASSIGNMA       AIR    VAULT
ASSIGNMA      LEAD      PB1
ASSIGNMA      LEAD      PB2
ASSIGNMA      LEAD      PB3
ASSIGNMA      LEAD      PB4
ASSIGNMA    VACUUM   BMLINE
ASSIGNMA    VACUUM     VOID
ASSIGNMA      LEAD      PB5
ASSIGNMA   Boron-po    POLY1
ASSIGNMA   Boron-po    POLY2
ASSIGNMA   Boron-po    POLY3
ASSIGNMA   Boron-po    POLY4
ASSIGNMA   Boron-po    POLY5
ASSIGNMA   Stainles    BLKHD
BIASING       0.0       1.    .0001   BMLINE
BIASING       0.0       1.    .0001    PIPE
BIASING       0.0       1.    .0005     PB1
BIASING       0.0       1.    .0025     PB2
BIASING       0.0       1.    .0125     PB3
BIASING       0.0       1.    .0625     PB4
BIASING       0.0      1.0     .3125     PB5
BIASING       0.0      1.0    1.5625    POLY1
BIASING       0.0      1.0    7.8125    POLY2
BIASING       0.0      1.0   39.0625    POLY3
BIASING       0.0      1.0   195.313    POLY4
BIASING       0.0      1.0   976.563    POLY5
BIASING       0.0      1.0   976.563    VAULT
BIASING       0.0      1.0   976.563    BLKHD
BIASING       0.0       1.   976.563   AIRGAP
BIASING       0.0       1.   976.563     VOID
BIASING       0.0      1.0   1953.13   DET1_1
BIASING       0.0      1.0   3906.25   DET1_2
BIASING       0.0      1.0    7812.5   DET1_3
BIASING       0.0      1.0   1953.13   DET2_1
BIASING       0.0      1.0   3906.25   DET2_2
BIASING       0.0      1.0    7812.5   DET2_3
STOP
```

F. LOCALIZED LEAD/BORATED-POLY/LEAD NONALTERNATING

```
* D:\Desktop\FLUKA inputs\pbbplypbnonalt.dat
* Created: 6.10.2011
* At: 23:59:29
PB-BPLY-PB-NONALT
MC-CAD Test
GLOBAL        1000.0       0.0       0.0       0.0       1.0
BEAM            -.1       0.0      30.0        .3       0.0      -1.0ELECTRON
BEAMPOS          0.0       0.0      -50.       0.0       0.0
AUXSCORE     USRBIN                    dose      dose         AMB74
USRBIN          11.   DOSE-EQ      -23.       50.       0.0   481.635dose
USRBIN          0.0       0.0   451.635       50.       36.       30.&
USRBIN          11.   DOSE-EQ      -27.   161.635       0.0      330.dose$
USRBIN       131.635       0.0      230.       50.       36.       30.&
USRBIN          11.     E+&E-      -24.       50.       0.0   481.635det-e
USRBIN          0.0       0.0   451.635       50.       36.       30.&
USRBIN          11.  EM-ENRGY      -25.       50.       0.0   481.635det-em
USRBIN          0.0       0.0   451.635       50.       36.       30.&
USRBIN          11.   NEUTRON      -26.       50.       0.0   481.635det-n
USRBIN          0.0       0.0   451.635       25.       36.       15.&
USRBIN          11.  EM-ENRGY      -21.      180.       0.0      490.det-em
USRBIN          0.0       0.0     -275.      100.       36.      250.&
USRBIN          11.   NEUTRON      -22.      180.       0.0      490.det-n
USRBIN          0.0       0.0     -275.      100.       36.      250.&
START        100000.
PHOTONUC         1.                    LEAD
PHOTONUC         1.                  POLYETHY
PHOTONUC        0.0                    WATER
GEOBEGIN                                                COMBNAME
    0    0               MC-CAD
* blkhole
SPH blkhole    0.00 0.00 0.00 100000.00
* out_blkhd
RCC outblkhd   0.00 0.00 -250.635 0.00 0.00 701.27 130.635
* in_blkhd
RCC in_blkhd   0.00 0.00 -250. 0.00 0.00 700. 130.
* pipe_in
RCC pipe_in    0.00 0.00 -99.75 0.00 0.00 400. 2.25
* pipe_out
RCC pipe_out   0.00 0.00 -100. 0.00 0.00 400.5 2.50
* void
SPH void       0.00 0.00 0.00 10000.00
RCC det1_1     0.0 0.0 451.635 0.0 0.0 10. 50.
RCC det1_2     0.0 0.0 461.635 0.0 0.0 10. 50.
RCC det1_3     0.0 0.0 471.635 0.0 0.0 10. 50.
RCC det2_1     0.0 0.0 230. 0.0 0.0 100. 131.635
RCC det2_2     0.0 0.0 230. 0.0 0.0 100. 141.635
RCC det2_3     0.0 0.0 230. 0.0 0.0 100. 151.635
RCC det2_4     0.0 0.0 230. 0.0 0.0 100. 161.635
RCC extra1     0.0 0.0 -100. 0.0 0.0 468. 70.
RCC extra2     0.0 0.0 -100. 0.0 0.0 475.5 77.5
```

```
RCC poly4      0.0 0.0 -100. 0.0 0.0 460.5 62.5
RCC poly3      0.0 0.0 -100. 0.0 0.0 453. 55.
RCC poly2      0.0 0.0 -100. 0.0 0.0 445.5 47.5
RCC poly1      0.0 0.0 -100. 0.0 0.0 438. 40.
RCC pb4        0.0 0.0 -100. 0.0 0.0 430.5 32.5
RCC pb3        0.0 0.0 -100. 0.0 0.0 423. 25.
RCC pb2        0.0 0.0 -100. 0.0 0.0 415.5 17.5
RCC pb1        0.0 0.0 -100. 0.0 0.0 408. 10.
END
* BLACKHOLE REGION OUTSIDE VOID
BLKHOLE      5 +blkhole  -void
* PIPE
PIPE         5 +pipe_out  -pipe_in
PB1          5 +pb1 -pipe_out
PB2          5 +pb2 -pb1
PB3          5 +pb3 -pb2
PB4          5 +pb4 -pb3
extra1       5 +extra1 -poly4
extra2       5 +extra2 -extra1
* VAULT
VAULT        5 +in_blkhd -extra2
* INSIDE BEAM PIPE
BMLINE       5 +pipe_in
* VOID REGION OUTSIDE TRAILER WALL
VOID         5 +void -outblkhd  -det1_1 -det1_2 -det1_3 -det2_1 -det2_2 -det2_3 -det2_4
* 1ST 5CM OF WATER DETECTOR
DET1_1       5 +det1_1
* 2ND 5CM OF WATER DETECTOR
DET1_2       5 +det1_2
* 3RD 5CM OF WATER DETECTOR
DET1_3       5 +det1_3
* 1ST 5CM OF WATER DETECTOR
DET2_1       5 +det2_2 -det2_1
* 2ND 5CM OF WATER DETECTOR
DET2_2       5 +det2_3 -det2_2
* 3RD 5CM OF WATER DETECTOR
DET2_3       5 +det2_4 -det2_3
* WALL OF TRAILER
BLKHD        5 +outblkhd -in_blkhd
* AIRGAP BETWEEN SIDE DETECTOR AND WALL
AIRGAP       5 -outblkhd +det2_1
POLY1        5 +poly1 -pb4
POLY2        5 +poly2 -poly1
POLY3        5 +poly3 -poly2
POLY4        5 +poly4 -poly3
END
GEOEND
ASSIGNMA      WATER    DET1_1
ASSIGNMA      WATER    DET1_2
ASSIGNMA      WATER    DET1_3
ASSIGNMA      WATER    DET2_1
ASSIGNMA      WATER    DET2_2
```

```
ASSIGNMA      WATER    DET2_3
ASSIGNMA     VACUUM    AIRGAP
* Concrete
* Concrete has a wide variation in density and composition. The above
* description is for poured structural concrete with 10% moisture
* content. Concrete block will have a density of about 2.05 g/cm3.
* Ranges of concrete composition are : C (8–25%), O (38–60%), Si (8–18%).
* Concrete composition can be analyzed cheaply by commercial laboratories.
MATERIAL                      2.34                       Concrete
COMPOUND       23.0    CARBON      40.0    OXYGEN      12.0   SILICONConcrete
COMPOUND       12.0   CALCIUM      10.0  HYDROGEN       2.0  MAGNESIUConcrete
MATERIAL        24.   51.9961      7.18                      CHROMIUM
* Stainless-Steel (typical)
* Stainless-Steel is produced with Cr content ranging from
* 4 - 19 Atomic Percent, and with C content from 0 - 4 percent.
MATERIAL                      8.0                        Stainles
COMPOUND       18.0  CHROMIUM      74.0      IRON       8.0    NICKELStainles
MATERIAL        5.    10.811      2.34                     BORON
* Boron-Poly
* SWX-210
MATERIAL                      1.12                       Boron-po
COMPOUND      -8.54  HYDROGEN     -30.0     BORON     -59.25    CARBONBoron-po
COMPOUND       -.76    OXYGEN     -1.01   SILICON     -0.38      IRONBoron-po
ASSIGNMA    BLCKHOLE   BLKHOLE
ASSIGNMA    Stainles      PIPE
ASSIGNMA       AIR     VAULT
ASSIGNMA      LEAD       PB1
ASSIGNMA      LEAD       PB2
ASSIGNMA      LEAD       PB3
ASSIGNMA    Boron-po       PB4
ASSIGNMA     VACUUM    BMLINE
ASSIGNMA     VACUUM      VOID
ASSIGNMA    Boron-po     POLY1
ASSIGNMA    Boron-po     POLY2
ASSIGNMA    Boron-po     POLY3
ASSIGNMA    Boron-po     POLY4
ASSIGNMA      LEAD    extra1
ASSIGNMA      LEAD    extra2
ASSIGNMA    Stainles     BLKHD
BIASING        0.0       1.     .0001    BMLINE
BIASING        0.0       1.     .0001     PIPE
BIASING        0.0       1.     .0005      PB1
BIASING        0.0       1.     .0025      PB2
BIASING        0.0       1.     .0125      PB3
BIASING        0.0       1.     .0625      PB4
BIASING        0.0      1.0      .3125    POLY1
BIASING        0.0      1.0     1.5625     POLY2
BIASING        0.0      1.0     7.8125     POLY3
BIASING        0.0      1.0   39.0625      POLY4
BIASING        0.0      1.0   195.313     extra1
BIASING        0.0      1.0   976.563     extra2
BIASING        0.0      1.0   976.563      VAULT
```

```
BIASING      0.0     1.0   976.563    BLKHD
BIASING      0.0      1.   976.563   AIRGAP
BIASING      0.0      1.   976.563     VOID
BIASING      0.0     1.0   1953.13   DET1_1
BIASING      0.0     1.0   3906.25   DET1_2
BIASING      0.0     1.0    7812.5   DET1_3
BIASING      0.0     1.0   1953.13   DET2_1
BIASING      0.0     1.0   3906.25   DET2_2
BIASING      0.0     1.0    7812.5   DET2_3
STOP
```

THIS PAGE INTENTIONALLY LEFT BLANK

LIST OF REFERENCES

[1] "Laser," [Online]. Available: http://en.wikipedia.org/wiki/Laser. [Accessed: July 10, 2011].

[2] W. B. Colson and A. M. Sessler, "Free Electron Lasers," *Annual Review of Nuclear and Particle Science,* vol. 35, pp. 25–54, December 1985.

[3] SETI Institute, "Free Electron Laser Communication – Bill Colson," [Video online]. Available: http://www.youtube.com/watch?v=4Vu-xiZOahQ

[4] W.B. Colson, "Free Electron Laser Physics," class notes for PH4055, Department of Physics, Naval Postgraduate School, summer 2011.

[5] T. C. Katsouleas et al*.,* "Scientific Assessment of High-Power Free-Electron Laser Technology for Naval Applications," in *The National Academies Press*, Washington, D.C., 2009.

[6] B. M. Dunham et al., "Performance of a Very High Voltage Photoemission Electron gun for a High Brightness, High Average Current ERL Injector," in *Proceedings of PAC07*, Albuquerque, New Mexico, 2007, pp. 1224–1226.

[7] W. B. Colson, "Free Electron Lasers," class notes for PH 4858, Department of Physics, Naval Postgraduate School, Fall 2009.

[8] J. Rathke et al., "Design and Fabrication of an FEL Injector Cryomodule," in *Proceedings of 2005 Particle Accelerator Conference Proceedings*, Knoxville, TN, pp. 3724–3726, 2005.

[9] Centre Laser Infrarouge d'Orsay, "What is a free electron laser?" [Online]. Available: http://clio.lcp.u-psud.fr/clio eng/FELrad.html. [Accessed: March 8, 2011].

[10] DESY Photon Science, "Low-Gain FEL with an Optical Cavity" [Online]. Avaliable:http://hasylab.desy.de/facilities/flash/machine/how_it_works/low_gain_fel /index_ eng.html. [Accessed: March 8, 2011].

[11] W. B. Colson, C. Pellegrini, A. Renieri, "Classical Free Electron Laser Theory," in *Free Electron Laser Handbook,* vol. 6, ch. 5. North-Holland Physics, 1990.

[12] Committee on a Scientific Assessment of Free-Electron Laser Technology for Naval Applications, National Research Council, *Scientific Assessment of High-Power Electron Laser Technology.* The National Academies Press, 2009, p. 30.

[13] I. Haber et al., "Measurement and simulation of source-generated halos in the University Of Maryland Electron Ring (UMER)," in *Particle Accelerator Conference, PAC. IEEE*, pp. 3564–3566, 25–29 June 2007

[14] Professor W. B. Colson (private communication), 2011.

[15] U.S. Nuclear Regulatory Commission, "Units of Dose," http://www.nrc.gov/reading-rm/ doc-collections/cfr/part020/part020–1004.html. [Accessed: October 2011].

[16] N. J. Carron, *An Introduction to the Passage Energetic Particles through Matter*. Boca Raton, FL: CRC Press, 2007.

[17] "Radiation Protection for Particle Accelerator Facilities," National Council on Radiation Protection and Measurements, NCRP Report No. 144, 2005.

[18] "Bremsstrahlung." In *Wikipedia,* http://en.wikipedia.org/wiki /File: Bremsstrahlung.svg. [Accessed: October 2011].

[19] J. Cossairt, "Radiation Physics for Personnel and Environmental Protection," Fermi National Accelerator Laboratory, Fermilab Report TM-1834. Rev 9B, May 2007. pp. 49–54.

[20] S. H. Ronki and W. R. Nelson, "The Electromagnetic Cascade shower," August 2, 2001. Available: http://www2.slac.stanford.edu/vvc/egs/lab/emshower.pdf.

[21] *Radiation Safety Manual.* Environmental Health and Safety, Stanford University, March 2010.

[22] G. Battistoni et al., "The FLUKA code: Description and benchmarking," *Proceedings of the Hadronic Shower Simulation Workshop 2006, Fermilab 6–8 September 2006, M. Albrow, R. Raja eds., AIP Conference Proceeding,* Vol. 896, pp. 31–49, 2007.

[23] A. Fasso` et al., "FLUKA: A Multi-Particle Transport Code," CERN-2005–10, INFN/TC_05/11, SLAC-R-773, 2005.

[24] X. K. Maruyama et al. "Measurement of Off-Axis Energy Deposition from 100 MeV Electrons Traversing Water and Liquid Nitrogen," *IEEE Transactions on Nuclear Science*, vol. 35, no. 6, December 1998.

[25] Sheildwerx, “SWX-210(30% Boron-Poly) Properties and Radiation Thickness Calculator,” July 2008, http://www.deqtech.com/Shieldwerx/Info/SWX-210_Radiation_Properties.pdf

THIS PAGE INTENTIONALLY LEFT BLANK

INITIAL DISTRIBUTION LIST

1. Defense Technical Information Center
   Ft. Belvoir, Virginia

2. Dudley Knox Library
   Naval Postgraduate School
   Monterey, California

3. Admiral Nevin Carr
   Office of Naval Research
   Arlington, Virginia

4. CDR(SEL) Sean Niles
   Office of Naval Research
   Arlington, Virginia

5. Quentin Saulter
   Office of Naval Research
   Arlington, Virginia

6. Sarwat Chappell
   Office of Naval Research
   Arlington, Virginia

7. Roger McGinnis
   Office of Naval Research
   Arlington, Virginia

8. Sarwat Chappell
   Office of Naval Research
   Arlington, Virginia

9. Michael Deitchman
   Office of Naval Research
   Arlington, Virginia

10. Prof. William B. Colson
    Naval Postgraduate School
    Monterey, California

11. Prof. Keith Cohn
    Naval Postgraduate School
    Monterey, California